ENERGY, EXERGY AND ENVIROMENTAL ASSESSMENT OF A NOVEL MULTI-GENERATION SYSTEM FED BY BIOMASS AND GEOTHERMAL ENERGY SOURCES

A Thesis Submitted to
the Graduate School of Engineering and Sciences of
Izmir Institute of Technology
in Partial Fulfillment of the Requirements for the Degree of

MASTER OF SCIENCE

in Energy Engineering

by
Utku ŞEKER

December 2022
İZMİR

ACKNOWLEDGEMENTS

I would like to express my sincere regards to my advisor and co-advisor Prof. Dr. Gulden G. Akkurt and Assoc. Prof. Dr. Mousa Mohammadpourfard-Tebriz University/Iran for their continuous support, motivation, and immense knowledge. Thanks to them, we have come to the end of this study by learning to approach problems from a different perspective.

My special thanks also go to Muhammad Hadi Taheri, who is PhD student in Tabriz University/Iran. I would like to thank him, whose support I always felt throughout a year journey, and who supported me to produce alternative solutions to the problems encountered and providing me a guidance.

I would like to thank the Bosch Thermotechnology family and my managers Zeynep Tezcan Arslantaş, Erkin Kocabaş and Burak Öztürk and many who supported my MSc. studies, believed in me, and provided support for the master courses and thesis study.

ABSTRACT

ENERGY, EXERGY AND ENVIROMENTAL ASSESSMENT OF A NOVEL MULTI-GENERATION SYSTEM FED BY BIOMASS AND GEOTHERMAL ENERGY SOURCES

Energy is the one of the critical tools that ensure the development of the countries. Since almost no country is completely energy independent, it is very important for countries to use the available energy efficiently and to produce their own energy from renewable energy sources. Multi-generation systems combine various cycles and processes to produce number of outputs and valuable market products using one or multiple energy sources as input. By creating a multi-generation system powered by renewable sources can increase system efficiency and provide some additional outputs such as hydrogen, heating, cooling, and domestic hot water. In this thesis, a novel multi-generation system consisting of a biomass gasification cycle, a double-flash geothermal cycle, an Organic Rankine Cycle and a PEM electrolyzer subsystems, is proposed to increase the efficiency and energy production from biomass and geothermal energy sources instead of using a single source for a single output. The proposed system is analyzed in terms of energy, exergy, and environmental impact point of view. By performing parametric studies for biomass flow rate, turbine inlet temperature, and single-objective optimization, effects on thermodynamic behavior and environmental impact are investigated for subsystems and overall system. The best operating conditions are determined. The findings indicate that energy efficiency of the proposed multi-generation system is 75% higher than a double-flash geothermal power plant. Based on the parametric study, biomass mass flow rate is encountered as the most significant parameter, which caused an 11.7% increase in energy efficiency, and 225% increase in environmental impact cost.

ÖZET

BİYOKÜTLE VE JEOTERMAL ENERJİ KAYNAKLI YENİ BİR ÇOKLU ÜRETİM SİSTEMİNİN ENERJİ, EKSERJİ VE ÇEVRESEL ANALİZİ

Enerji, ülkelerin kalkınmasını sağlayan kritik araçlardan biridir. Hemen hemen hiçbir ülke enerjiden tamamen bağımsız olmadığı için ülkelerin mevcut enerjiyi verimli kullanmaları ve yenilenebilir enerji kaynaklarından kendi enerjilerini üretmeleri çok önemlidir. Çoklu üretim sistemleri, girdi olarak bir veya daha fazla enerji kaynağı kullanarak çok sayıda çıktı ve değerli pazar ürünleri üretmek için çeşitli döngüleri ve süreçleri bir araya getirir. Girdi olarak yenilenebilir enerji kaynakları kullanılan bir çoklu üretim sistemi ile sistem verimliliği artırılabilir,ve hidrojen, ısıtma, soğutma ve kullanım sıcak suyu gibi bazı ek çıktılar sağlanabilir. Bu tezde, bir biyokütle gazlaştırma çevrimi, bir çift buharlaştırmalı jeotermal çevrim, bir Organik Rankine Çevrimi ve bir PEM elektrolizörü alt sistemlerinden oluşan yeni bir çoklu üretim sistemi tasarlanmıştır. Enerji kaynağı olarak biyokütle ve jeotermal enerji kaynaklarının kullanıldığı bu sistem ile tek enerji kaynaklı ve tek çıktılı bir sisteme göre enerji üretimi ve verimliliği artırmak amaçlanmaktadır. Önerilen sistem; enerji, ekserji ve çevresel etki açısından analiz edilmiştir. Biyokütle debisi ve türbin giriş sıcaklığı için parametrik bir çalışmanın yanısıra tek amaçlı optimizasyon çalışması yapılarak, alt sistemler ve sistem genelinde termodinamik davranış ve çevresel etki üzerindeki etkiler araştırılmış, en iyi çalışma koşulları belirlenmiştir. Bulgular, önerilen çoklu üretim sisteminin enerji verimliliğinin, çift buharlaştırmalı bir jeotermal enerji santralinden %75 daha yüksek olduğunu göstermektedir. Parametrik çalışmaya göre, enerji verimliliğinde %11,7'lik artışa ve çevresel etki maliyetinde %225'lik bir artışa neden olan biyokütle debisi en etkili parametredir.

TABLE OF CONTENTS

LIST OF FIGURES

Figure **Page**

LIST OF TABLES

Table **Page**

LIST OF SYMBOLS

A	Area (m^2)
$\dot{C}$	Cost rate ($/yr)
$\dot{E}x$	Exergy rate (kW)
F	Faraday constant (c/mol)
h	Enthalpy (kJ/kg)
J	Current density (A/m^2)
$\dot{m}$	Mass flow rate (kg/s)
η_{en}	Energy efficiency
η_{ex}	Exergy efficiency
η_s	Isentropic efficiency
$\dot{Q}$	Heat transfer rate (kW)
R	Gas Constant (J/mol K)
s	Specific entropy (kJ/kg.K)
T	Temperature (°C)
$\dot{W}$	Power (kW)

SUBSCRIPTS

0	Environmental state
A	Anode
Ac	Air compressor
Act	Activation
C	Cathode
Ch	Chemical
D	Destruction
Gt	Gas turbine
En	Energy
Ev	Expansion valve
Ex	Exergy
Hps	High pressure seperator
In	Inlet
Is	Isentropic
Lps	Low pressure seperator
Ph	Physical
Pu	Pump
Tur	Turbine

LIST OF ABBREVIATIONS

DFG	Double-flash Geothermal
EES	Engineering Equation Solver
GHG	Greenhouse Gas
GT	Gas Turbine
HEX	Heat Exchanger
IHE	Internal Heat Exchanger
LMTD	Logarithmic Mean Temperature Difference
LHV	Latent Heat of Vaporization
ORC	Organic Rankine Cycle
RO	Reverse Osmosis
SGPP	Sabalan Geothermal Power Plant
TIT	Turbine Inlet Temperature
PEM	Proton Exchange Membrane

CHAPTER 1

INTRODUCTION

Increased demand in energy consumption is strongly linked to global population growth, economic development, and human well-being. By 2040, the World's energy demand and the share of renewable energy production are expected to grow by more than 25% and 40% from today's level, respectively. Based on the global targets set by the Paris Agreement, many countries committed to reduce greenhouse gas emissions by 45% by 2030 and reach net zero by 2050 [1,2]. To be able to achieve these targets, multi-generation systems powered by renewable energy sources are considered as one of the key solutions. Multi-generation systems provide higher efficiency, lower/zero carbon emissions and lower cost. The primary energy sources that used to generate power are still fossil fuels. Natural gas is the most common one, contributing around 36.7% of global power generation, as shown in Fig.1.1 [3].

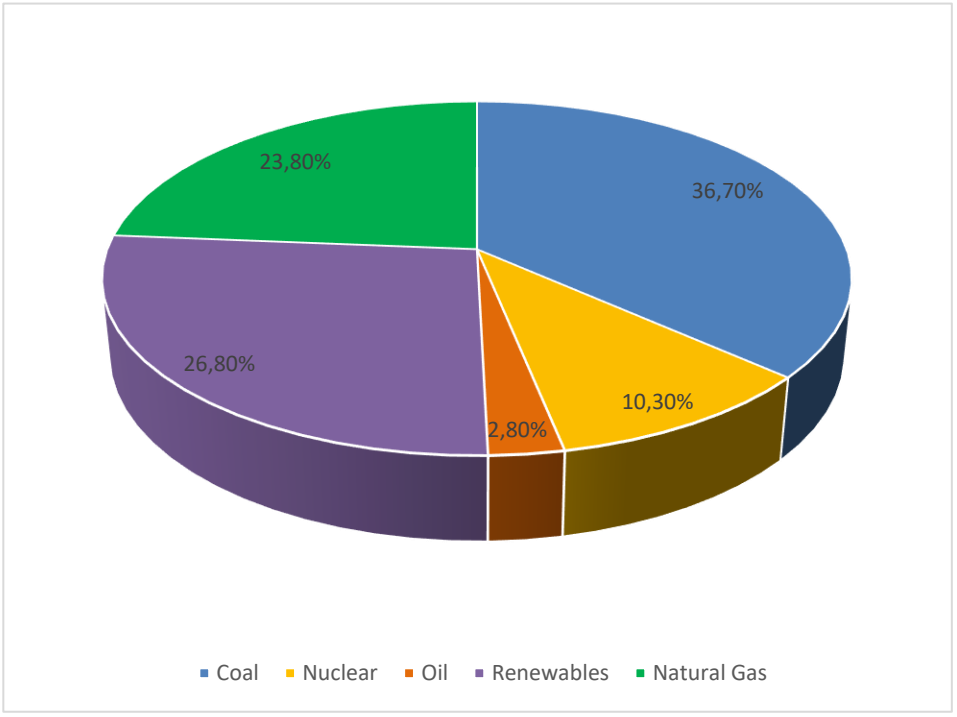

Figure 1.1. The share of energy resources on power generation in the World [3].

The contribution of renewable energy sources to the power mix increasing year by year. Biomass and hydropower are the most widely available renewable energy sources with a total share of 85% as can be seen from Fig.1.2 [4]. The share of wind, geothermal and solar energy is 15%.

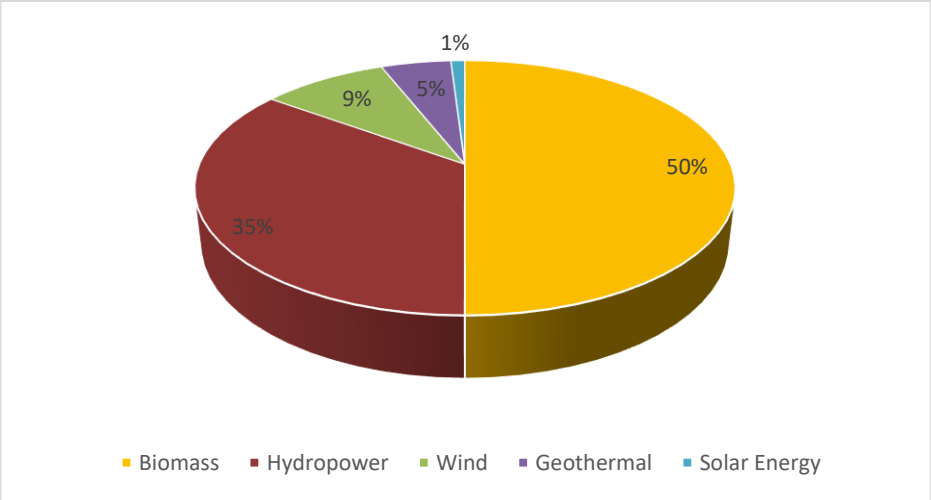

Figure 1.2. Availability of renewable energy sources in the World [4].

Multi-generation is a way of producing energy and valuable market products by power generation cycles and processes reducing amount of waste heat and carbon emissions, and increasing efficiency over single-generation systems. If powered by renewable energy sources, the impact on environment and cost effectiveness of multi-generation systems will increase. Comparing with single-generation systems multi-generation systems produces power and additional products such as hydrogen, heating/cooling, desalinated water, hot water, etc. The overall efficiency of conventional power plants operating on a single source using fossil fuels is mainly below 40%. That means, more than 60% of the heating value of the fuel entering a conventional power plant is lost in the form of waste heat and mechanical losses [5]. Multi-generation systems use the waste heat to produce more power and other products. Therefore, conventional power plants need more energy input to produce the same power output as multi-generation systems, increasing operating costs [5].

One of the areas studied on energy systems in general is optimization. In energy systems, it is desired to keep the benefit maximum and the expenses minimum. The benefit is generally based on work/heat output, and energy-exergy efficiency. In order to

apply optimization techniques to any system, the mathematical model of the system must be created and the parameters to be optimized must be defined.

Biomass gasification is one of the thermochemical processes that converts biomass to syngas to be used as an energy carrier. Furthermore, gasification is one of the best alternative solutions due to natural gas price volatility and environmental concerns. Since biomass sources are converted to syngas, it is easy to store and use in multi-generation systems. Syngas includes hydrogen (H_2), carbon monoxide (CO), methane (CH_4), water vapor (H_2O), carbon dioxide (CO_2), nitrogen (N_2), and other gases [5]. Gasification process has significantly higher efficiency than biomass combustion process. The research community is concentrating on the design and analysis of efficient integration of biomass gasification with other renewables to power multi-generation systems.

Electricity is generated by conversion technologies from geothermal fluids even at low temperatures with a history of more than 100 years. Since geothermal resources are not affected from weather conditions, they are considered as the most reliable renewable energy source. Geothermal energy, which has been used widely for almost a century, is expected to grow. In 2050, geothermal resources are forecasted to provide 3% of the World energy supply [6]. It is advantageous to implement these resources as a subsystem to the multi-generation systems along with biomass process. Biomass gasification provides additional heat to the geothermal cycle and a good match of heat range. Energy, exergy, and environmental impact (3E) assessment are conducted by Engineering Equation Solver (EES) [18] for the multi-generation system alternatives developed in the thesis, and the final system configuration is decided. The final multi-generation system consists of a biomass gasification cycle (BGC), a double-flash geothermal (DFG) cycle, an Organic Rankine Cycle (ORC) and a Proton Exchange Membrane (PEM) electrolyzer to produce hydrogen. Furthermore, a single-objective optimization is executed in the EES to determine the best operating conditions in terms of energy, exergy, and the environment impact.

1.1. Motivation

Development level of the countries is directly linked with available energy production. Producing safe and environmentally friendly methods are crucial. While multi-generation systems are gaining importance day by day instead of single output/conventional plants. Izmir-Türkiye has a high geothermal energy potential. Since geothermal resources mostly located at rural areas where agricultural activities are also

high, makes geothermal and biomass a good couple. In this thesis, a multi-generation system is proposed by considering renewable energy source availability of Izmir-Türkiye to show possible benefits.

1.2. Thesis Overview

The thesis is composed of 5 chapters. Chapter 2 gives a through literature survey and points out the research gaps on multi-generation systems. The chapter also includes the recent studies about subsystems which are used in the thesis study.

The third chapter covers the materials and methods section. Proposed multi-generation system and all used subsystems are defined. Furthermore, the equations for thermodynamic analysis of each subsystem are given. Finally, environmental impact assessment analysis and single-objective optimization methods are presented.

Results are presented and discussed in Chapter 4. Lastly, Chapter 5 presents conclusions and recommendations for future studies.

CHAPTER 2

LITERATURE REVIEW

Literature review is mainly focused on multi-generation systems powered by geothermal energy, combination with other renewables and biomass energy for power generation and hydrogen production.

Since geothermal energy is one of the most sustainable energy sources, it is a widely used energy source in multi-generation systems. Mohammadzadeh Bina et al. (2018) analyzed the performance of single and DFG power plants at Sabalan Geothermal Field-Iran. Studies shows that double flash has higher energy efficiency 10% compared to single flash 7.3% [20].

Furthermore, Koc et al. (2022) applied an energy, exergy, exergo-economic analysis their proposed multi-generation plant driven by geothermal energy [32]. Plant performance is analyzed based on working parameters. They targeted to provide hydrogen, electricity, heating, cooling, and swimming pool heating with this multi-generation plant. According to applied thermodynamic analysis energy and exergy efficiencies were calculated as 32.3% and 25.4%, respectively. Furthermore, the effect of geothermal temperature and mass flow rate change on the system performance was studied.

Moreover, there are several examples which combine geothermal energy with solar energy. For instance, Ozturk and Dincer (2020) carried out a thermodynamic analysis of a solar and geothermal-based multi-generation system with hydrogen production. They designed their configuration to produce six output which are power, cooling, heating, drying air, hydrogen and domestic hot water [29]. The exergy efficiency and exergy destruction rate for the subsystems and the overall system show that parabolic collectors have the highest exergy destruction rate among the components of the solar based multi-generation system. System energy and exergy efficiencies reached 75.1% and 52.3% using multi-generation system benefits respectively.

Biomass is another commonly available renewable energy source which is used in to drive a high amount of multi-generation systems in the literature. Ahmadi et al. (2013) proposed and thermodynamically evaluated a new multi-generation system based on a

biomass burner, an ORC, an absorption cooling system, a PEM electrolyzer to produce hydrogen, and a domestic water heater for hot water production. Exergy analysis was performed to identify irreversibility's in each component and system performance. In addition, they conducted an environmental impact assessment of the multi-generation system and examined the possible reduction in CO_2 emissions [30]. A parametric study was conducted to understand the system performance more comprehensively and to investigate the effects of important design parameters on the energy and exergy efficiency of the system. Due to the high temperature difference and combustion reaction, the exergy destruction calculations demonstrate the combustion chamber, and the ORC evaporator are the two significant points of irreversibility with the highest exergy destruction rate. Combustion chamber temperature, ORC turbine inlet pressure, and ORC pump inlet temperature are the key parameters that affect system performance.

Besides, there are several studies that combination of biomass and other renewable energy sources such as solar energy. Yuksel and Ozturk (2017) performed an energy and exergy analysis of the multi-generation solar and biomass-based energy system and performed a parametric study [31]. According to the results, they obtained that the combustion chamber and solar collector have the highest exergy destruction rate of the integrated process. Biomass and solar energy efficiencies are calculated separately as 24.0% and 28.5%, respectively. Besides, after integration of the biomass and solar efficiencies are increased 57.4% and 59.2%.

Furthermore, hydrogen is the one of the important valuable products. Since hydrogen is seen as a promising alternative to natural gas especially in Europe, scientific research accelerated and there has recently been a lot of focus on hydrogen production, which can be used as fuel in fuel cells. Solid oxide fuel cells (SOFC), proton exchange membrane fuel cells (PEMFC), molten carbonate fuel cells (MCFC), and phosphoric acid fuel cells are the four main types of fuel cells. Combining PEM systems with various power plants, particularly steam Rankine cycles and ORCs, has received a lot of attention in the literature due to its current density and compact concept [18].

According to the author's knowledge, there is no any study combining geothermal and biomass energy sources to drive a multi-generation system. To fill this gap, in this thesis, a novel multi-generation system which is driven by geothermal-biomass energy couple, is designed and analyzed to determine the possible improvements over single-generation geothermal based power generation systems. The proposed multi-generation system consists of a BGC, a DFG cycle, an ORC and a PEM electrolyzer.

CHAPTER 3

MATERIALS AND METHODS

In this thesis, a novel multi-generation system is proposed in which geothermal energy and biomass are used as the main energy input to produce electricity, and hydrogen. The flow diagram of the proposed system is illustrated in Fig.3.1. A detailed energy, exergy and environmental impact analysis are conducted by EES software for each subsystem and overall system. The key performance parameters, which are power generation rates, energy and exergy efficiencies, exergy destruction rates, hydrogen production rates, and the amount of CO_2 emissions, are calculated.

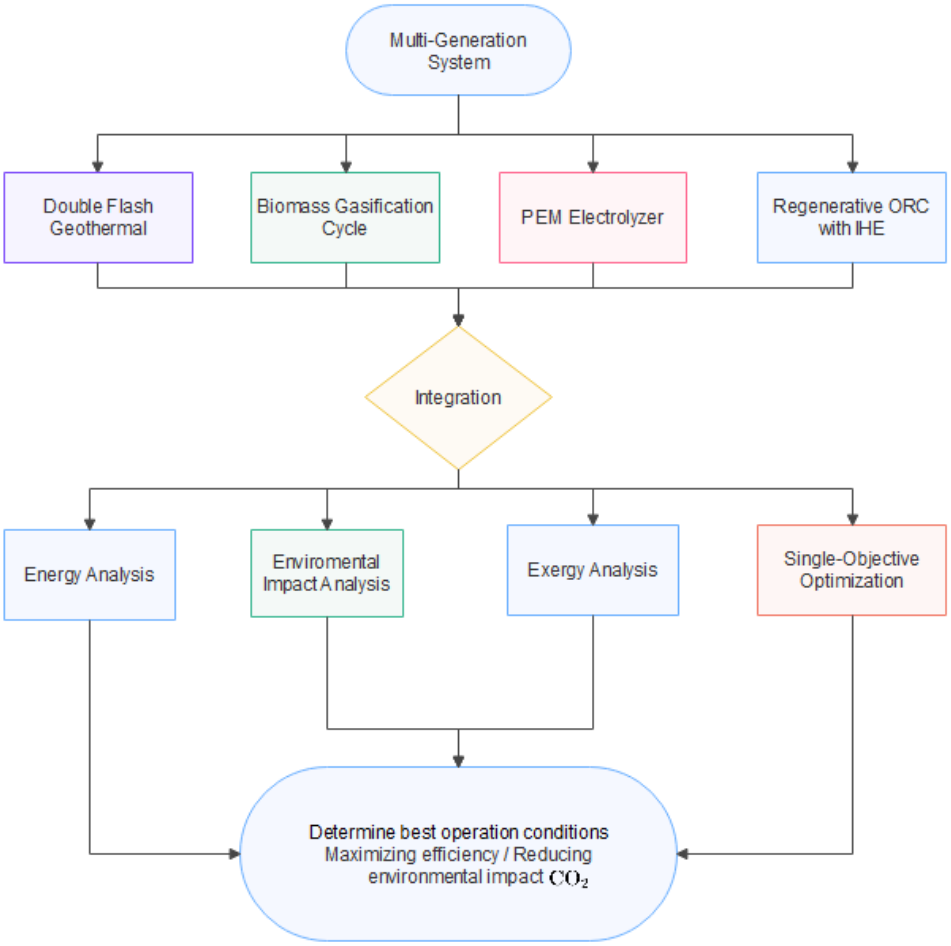

Figure 3.1. Flow diagram of the proposed system.

3.1 System Description

Fig.3.2. presents a block diagram of the proposed multi-generation system, which includes four subsystems as (1) a BGC, (2) a DFG cycle, (3) an ORC system with an internal heat exchanger (IHE), and (4) a PEM electrolyzer. The energy inputs of the system are biomass and geothermal energy while outputs are electricity, and hydrogen. Each subsystem is described in detail below.

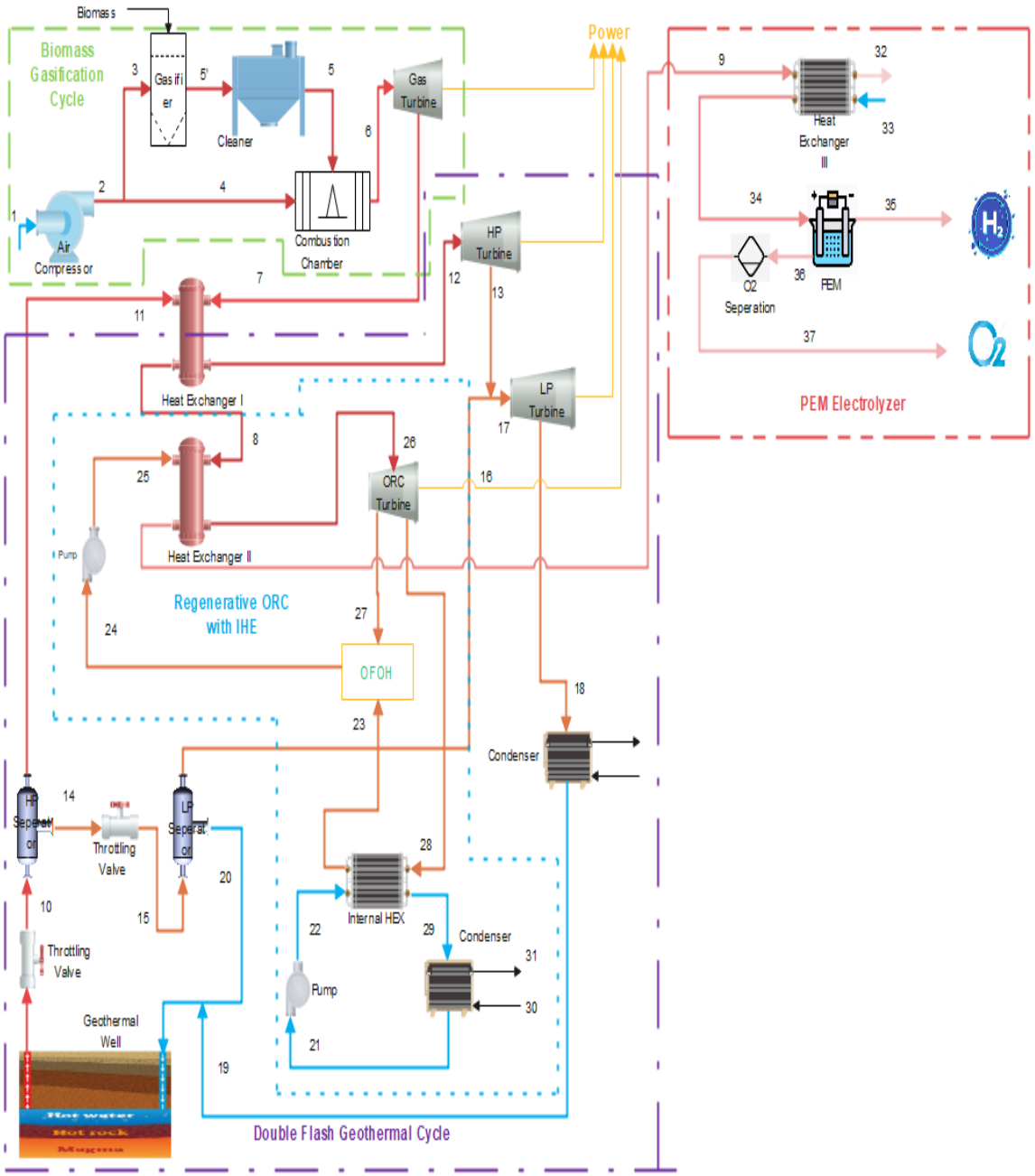

Figure 3.2. Block diagram of proposed multi-generation system.

3.1.1. Subsystem I: Biomass Gasification Cycle

The biomass enters the subsystem (between state 3-5') at ambient temperature and pressure. Air is compressed by a compressor (state 2) before it is fed into the gasifier unit (state 3), where the syngas is produced. The syngas is cleaned removing char and tar at the cleaner. Then, syngas is directed to the combustion chamber (state 5) and is burned by air at a predetermined mixture of air-fuel (state 4). The combustion products at high temperature and pressure are used in a gas turbine (GT) to generate power (state 6).

3.1.2. Subsystem II: Double-flash Geothermal Cycle

In this subsystem, geothermal fluid at the production well exists in two-phase. Since conventional geothermal power plants need steam to generate power, geothermal fluid passes through a throttling valve where a part of the liquid phase flashes into steam (state 10). Then, steam is separated (state 11) from liquid in a high pressure (HP) separator (state 14) and directed to a HP steam turbine. Liquid phase leaves the separator, still at high temperature, is flashes one more time to produce more steam (state 14). The mixture is separated into steam and liquid phases again at low pressure (LP) separator (state 16). This LP steam along with the stream of HP turbine exit is used to generate extra power at an LP turbine (state 17). Liquid phase at LP separator exit is re-injected back to the geothermal reservoir (state 19 and 20). High temperate flue gas at the gas turbine exit (Subsystem I) is used to increase geothermal steam temperature by a heat exchanger (HEX I) (state 12).

3.1.3. Subsystem III: Organic Rankine Cycle

Flue gas leaving the gas turbine, transfers its heat to geothermal steam at Subsystem II. Then, it moves to HEX II as a heat source of the ORC (state 8). Working fluid used in the cycle enters the HEX II as liquid and leaves as vapor which is used to generate power in a steam turbine (state 26). The expanded vapor is pre-cooled in the IHE and further cooled at open feed organic heater (OFOH). The OFOH component helps pre-heating of working fluid. This situation leads reducing irreversibilities and improves the thermodynamic efficiency of the system. Liquid-steam mixture at the turbine outlet flows to OFOH (state 27) and IHE (state 28). Steam is converted into liquid in the condenser

(state 29). Two pumps are implemented in the ORC cycle to stream of the working fluid (state 21 and 24).

3.1.4. Subsystem IV: PEM Electrolyzer

Last portion of the waste heat of flue gas (state 9) is used to increase water temperature in a PEM electrolyzer. Fresh water enters HEX III (state 33), absorbs heat from the flue gas and is used to produce hydrogen in PEM electrolyzer. The required electricity is provided from produced power by the multi-generation system.

3.2. Thermodynamic Analysis

Energy and exergy analysis are performed to calculate the thermodynamic states in order to evaluate power generation rates, energy and exergy efficiencies, exergy destruction rates, hydrogen production rates, and the amount of CO_2 emissions of the proposed multi-generation system and to determine the best operating conditions. Mass and energy conversion equations for steady-state, steady-flow operations are shown in Eq.1 and 2 [17].

$$\sum \dot{m}_{in} = \sum \dot{m}_{out} \quad \text{(kg/s)} \tag{1}$$

$$\dot{Q} - \dot{W} = \sum \dot{m}_{out}\,(h_{out}) - \sum \dot{m}_{in}\,(h_{in}) \quad \text{(kW)} \tag{2}$$

Maximum useful work is referred as exergy. Summation of physical and chemical exergy rates give each stream's total exergy rate is given in Eq.3 [17].

$$\dot{E} = \dot{E}_{ph} + \dot{E}_{ch} \quad \text{(kW)} \tag{3}$$

Physical exergy and chemical exergy rates are defined in Eq.4 and 5, respectively [17].

$$\dot{E}_{ph} = \dot{m}(h - h_0) - T_0(s - s_0)] \quad \text{(kW)} \tag{4}$$

$$\dot{E}_{ch} = \dot{m}[\Sigma y_i ex_i^{ch,o} + \bar{R}T_0 \Sigma y_i \ln(y_i)] \quad \text{(kW)} \tag{5}$$

The assumptions made for the thermodynamic analysis are;

- In all processes, energy and exergy balance are under steady-state, steady-flow conditions.

- Combustion products of biomass and air are ideal gases.
- Pressure drops in the heat exchangers and pipelines are ignored.
- The efficiencies of the turbines and pumps are assumed as isentropic.
- The changes in kinetic and potential energies are neglected.

3.2.1. Biomass Gasification Cycle

Table 3.1 shows the final analysis of the solid waste which is used as biomass material in the study. Chemical characteristics of solid waste is given in Table 3.1 [11]. Chemical reaction equation is expressed in the Eq.6.

Table 3.1. Characteristics of solid waste.

Properties	Unit	Value
Moisture content	(% by weight)	10
Latent heat of vaporization (LHV)	(kJ/kg)	25,021.51
Ultimate analysis (dry basis by weight)		
Carbon	(%)	51.03
Oxygen	(%)	39.17
Nitrogen	(%)	2.64
Hydrogen	(%)	6.77

$$\begin{aligned}&\left(\mathrm{C}_{a_1}\mathrm{H}_{a_2}\mathrm{O}_{a_3}\mathrm{N}_{a_4}\right)_{\text{ash free dry fuel}}+\left(a_5(\mathrm{O}_2+3.76\mathrm{N}_2)\right)_{\text{air}}\\&+\left(a_6\mathrm{H}_2\mathrm{O}_{(\text{gas})}\right)_{\text{steam}}+\left(a_7\mathrm{H}_2\mathrm{O}_{(\text{liquid})}\right)_{\text{moisture content}}\\&\Rightarrow\left(b_1\mathrm{CH}_4+b_2\mathrm{CO}+b_3\mathrm{CO}_2+b_4\mathrm{H}_2+b_5\mathrm{H}_2\mathrm{O}+b_6\mathrm{N}_2\right)_{\text{Syngas}}\end{aligned} \quad (6)$$

a_1, a_2, a_3, a_4 represents mole ratios of input chemical reaction which is given in Eq.6. Molecular weight calculation method is expressed in the Eq.7. Calculated mole ratios of Eq.6 are listed in Table 3.2.

$$a_2=\frac{(\chi_{\mathrm{H}}/M_{\mathrm{H}})}{(\chi_{\mathrm{C}}/M_{\mathrm{C}})},a_3=\frac{(\chi_{\mathrm{O}}/M_{\mathrm{O}})}{(\chi_{\mathrm{C}}/M_{\mathrm{C}})},a_4=\frac{(\chi_{\mathrm{N}}/M_{\mathrm{N}})}{(\chi_{\mathrm{C}}/M_{\mathrm{C}})} \quad (7)$$

a_5 is the required air mole ratio for gasification process of biomass. Besides, a_6 and a_7 can be calculated as given in Eq.8.

$$a_5 = \frac{\text{AFR} \times M_{\text{wet fuel}}}{M_{\text{air}}}, a_6 = \frac{\text{SAFR} \times M_{\text{wet fuel}}}{M_{\text{H}_2\text{O}}} \quad (8)$$

When gasifier reaches 12 bars, the fuel-air ratio and stoichiometric fuel-air ratio are obtained as 0.25 and 1, respectively. The mole balance equations for the described reaction are used to calculate syngas coefficients in air-steam gasification in Eq.6 and the equilibrium constant equation for both methane, water shift reaction to be solved. The constants used in Eq.6 is provided from [26] and listed in Table 3.2. $b_{1,2,3}$ represents moles of respective gas components.

Table 3.2. Coefficients of Eq.6 [26].

Coefficient	**Value**
a_1	1
a_2	1.6
a_3	0.58
a_4	0.044
a_5	0.277
a_6	1.45
a_7	0.145
b_1	0.1387
b_2	0.3162
b_3	0.55
b_4	0.795
b_5	1.32
b_6	1.06

In the combustion chamber, combustion occurs with syngas and air mixture. Air flow rate is set by turbine inlet temperature. Energy balance for combustion chamber is applied to calculate required air flow rate for a complete combustion. This equivalence is expressed in Eq.9.

$$(b_1\text{CH}_4 + b_2\text{CO} + b_3\text{CO}_2 + b_4\text{H}_2 + b_5\text{H}_2\text{O} + b_6N_2)_{\text{Syngas}} + \left(\beta(\text{O}_2 + 3.76\text{N}_2)\right)_{\text{air}} \Rightarrow (c_1\text{CO}_2 + c_2\text{H}_2\text{O} + c_3\text{O}_2 + c_4N_2)_{\text{Products}} \quad (9)$$

β is the coefficient of air, and other combustion coefficients of Eq.9 are given in Table 3.3.

Table 3.3. Coefficients of Eq.9 [26].

Coefficient	Value
c1	1
c2	2.392
c3	2.021
c4	11.79
β	2.854

The compressor and turbine exit temperatures can be calculated as given in Eq.10-11 [12]:

$$T_2/T_1 = 1 + \frac{1}{\eta_{s,\mathrm{AC}}}\left[\left(\frac{P_2}{P_1}\right)^{\frac{k-1}{k}} - 1\right] \tag{10}$$

$$T_7/T_6 = 1 - \eta_{s,\mathrm{GT}}\left[1 - \left(\frac{P_6}{P_7}\right)^{\frac{1-k}{k}}\right] \tag{11}$$

where $\eta_{s,AC}$, shows compressor isentropic efficiency and $\eta_{s,GT}$, denotes gas turbine isentropic efficiency, and k is the ratio of specific heat. Destruction of exergy definitions and correlations of energy and exergy efficiencies are listed in Table 3.4 and 3.5, respectively. BGC is given in the Fig.3.3.

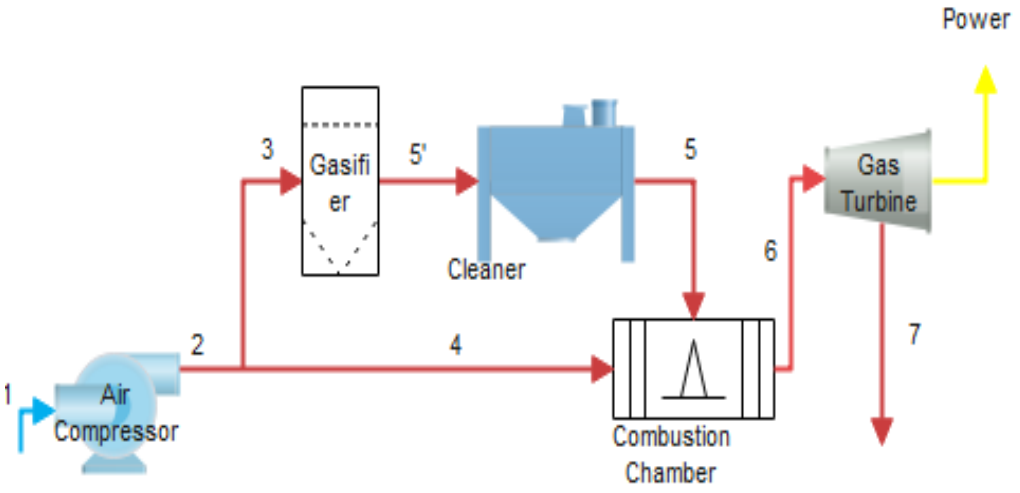

Figure 3.3. Schematic diagram of BGC [19].

Table 3.4. Exergy destruction definitions for BGC.

Component	Exergy Destruction Rate (kW)
Air compressor	$\dot{E}x_{D,AC} = \dot{W}_{AC} - \dot{E}x_2$
Gasifier	$\dot{E}x_{D.gasifier} = \dot{E}x_{biomass} + \dot{E}x_{16} + \dot{E}x_3 - \dot{E}x_{5'}$
Combustion chamber	$\dot{E}x_{D,\ combustion\ chamber} = \dot{E}x_4 + \dot{E}x_5 - \dot{E}x_6$
Gas turbine	$\dot{E}x_{D,GT} = \dot{E}x_6 - \dot{E}x_7 - \dot{W}_{GT}$

Table 3.5. Expressions for energy and exergy efficiencies.

BGC [27]	
Energy Efficiency (%)	**Exergy Efficiency (%)**
$\eta_{en,gasi} = \frac{\dot{W}_{GT} - \dot{W}_{AC}}{\dot{m}_{biomass}\ LHV_{biomass,dry}}$	$\eta_{ex,\ gasi} = \frac{\dot{W}_{GT} - \dot{W}_{AC}}{\dot{E}x_{biomass}}$

3.2.2. Double-flash Geothermal Cycle

In this part of the study, DFG cycle has been implemented into multi-generation power cycle based on the Sabalan geothermal field/Iran data. During thermodynamic analysis, the following assumptions have been made.

- The system operates under steady-state, steady-flow conditions.
- Pressure drops are not considered.
- The changes in kinetic and potential energy are neglected.
- Pressure and temperature of the wells are assumed to be constant during the process.
- Dead state properties are assumed as T_0 = 25°C and P_0 = 101 kPa.
- The efficiencies of the turbines and pumps are assumed as isentropic.

The thermodynamic equations are presented based on the first and second law of thermodynamics. Table 3.6 demonstrates first law of thermodynamics equations of the cycle.

Table 3.6. Equations of the DFG [13-15].

Component	Equation
Flash chamber I	$h_{10} = h_{11}$
HP-Cyclone separator	$x_{14} = \frac{h_{10} - h_{14}}{h_{11} - h_{14}}$
Flash chamber II	$h_{14} = h_{15}$

(Cont. on next page)

Table 3.6. (Cont.)

LP-Cyclone separator	$x_{16} = \frac{h_{15} - h_{20}}{h_{16} - h_{20}}$
High-pressure turbine	$\dot{W}_{T,HP} = \dot{m}_{12}(h_{12} - h_{13})$
	$\eta_{s,HP} = \frac{h_{12} - h_{13}}{h_{12} - h_{13s}}$
Low-pressure turbine	$\dot{W}_{T,LP} = \dot{m}_{17}(h_{17} - h_{18})$
	$\eta_{s,LP} = \frac{h_{17} - h_{18}}{h_{17} - h_{18s}}$
Condenser	$Q_{cond} = \dot{m}_{18}(h_{18} - h_{19})$

Thermodynamic irreversibilities of the system can be pinpointed by exergy analysis [16]. Table 3.7 lists exergy balance and exergy efficiency equations.

Table 3.7. Exergy efficiency equations and exergy destruction rate of DFG [17].

Component	**Exergy Destruction Rate (kW)**	**Exergy Efficiency (%)**
Expansion valve 1	$\dot{Ex}_{D,EV1} = T_0\dot{m}_{11}(s_{11} - s_{10})$	$\eta_{ex,EV1} = \frac{\dot{Ex}_{11}}{\dot{Ex}_{10}}$

(Cont. on next page)

Table 3.7. (Cont.)

HP-separator	$\dot{Ex}_{D,HPS} = \dot{Ex}_{10} - (\dot{Ex}_{11} + \dot{Ex}_{14})$	$\eta_{ex,HPS} = \frac{(\dot{Ex}_{11} + \dot{Ex}_{14})}{\dot{Ex}_{10}}$
Expansion valve 2	$\dot{Ex}_{D,EV2} = T_0 \dot{m}_{14}(s_{15} - s_{14})$	$\eta_{ex,EV2} = \frac{\dot{Ex}_{15}}{\dot{Ex}_{14}}$
LP-separator	$\dot{Ex}_{D,LPS} = \dot{Ex}_{15} - (\dot{E}x_{20} + \dot{E}x_{16})$	$\eta_{ex,LPS} = \frac{(\dot{Ex}_{20} + \dot{E}x_{16})}{\dot{E}x_{15}}$
HP turbine	$\dot{Ex}_{D,T,HP} = \dot{Ex}_{12} - \dot{E}x_{13} - \dot{W}_{T,HP}$	$\dot{Ex}_{D,T,HP} = \dot{Ex}_{12} - \dot{E}x_{13} - \dot{W}_{T,HP}$
LP turbine	$\dot{Ex}_{D,T,HP} = \dot{Ex}_{17} - \dot{E}x_{18} - \dot{W}_{T,LP}$	$\eta_{ex,T,HP} = \frac{\dot{W}_{T,LP}}{\dot{Ex}_{17} - \dot{E}x_{18}}$
Condenser	$\dot{Ex}_{D,\,\mathrm{cond}} = (\dot{E}x_6 - \dot{Ex}_7) - (\dot{Ex}_{13} - \dot{Ex}_{12})$	$\eta_{ex,cond} = \frac{(\dot{Ex}_{13} - \dot{Ex}_{12})}{(\dot{E}x_6 - \dot{E}x_7)}$
Reinjection	$\dot{Ex}_{D,r} = \dot{Ex}_{19} + \dot{Ex}_{20}$	-----

Mohammadzadeh Bina et al. (2018) were developed a DFG power plant (Fig.3.4) for Sabalan Geothermal Field-Iran and the plant was evaluated from thermodynamics point of view. In this subsystem of the thesis, the model is verified by the data of the Ref. [20]. The data for states as given in Fig.3.4, are listed in Table 3.8.

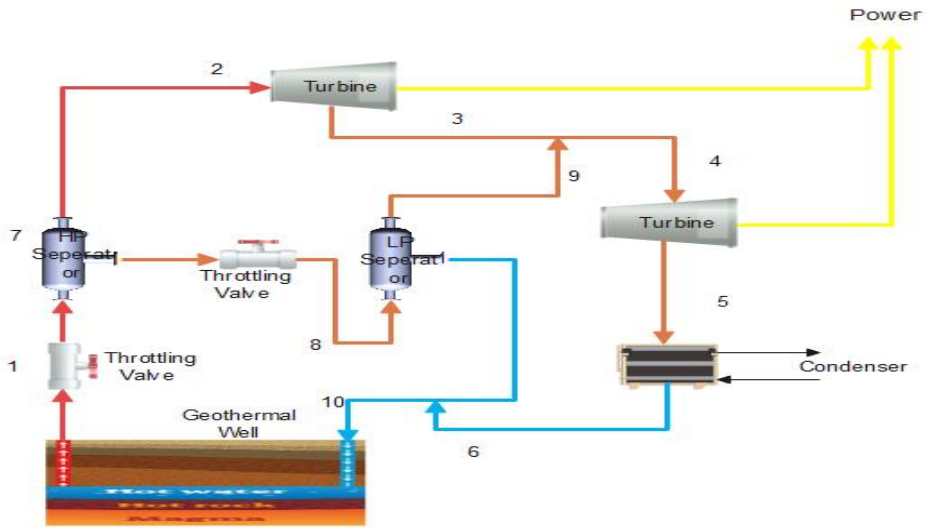

Figure 3.4. Schematic diagram of DFG cycle [20].

Table 3.8. Validated Sabalan Geothermal Field-Iran data [19-20].

State	$\dot{m}_i$ $\left(\frac{kg}{s}\right)$	T_i $(°C)$	h_i $\left(\frac{kJ}{kg}\right)$
1	285.0	237.9	1027.0
2	46.7	168.5	2766.0
3	43.7	101.2	2480.0
4	74.5	40.0	2562.0
5	74.5	40.0	2246 .0
6	74.5	168.5	167.5
7	241.3	101.3	712.3
8	241.3	101.3	712.3
9	30.8	101.3	2678.0
10	210.5	101.3	424.4

3.2.3. Organic Rankine Cycle

In this study, in terms of improving Rankine cycle efficiency, a regenerative cycle is implemented (Fig.3.5). The working fluid used in the cycle is chosen as R123 based on

a research article [14]. The author indicated that R123 performed best based on produced power, exergy destruction, first law efficiency and second law efficiency.

The mass, energy, and exergy balance equations of the ORC are given in Eq.s 12-14 [14].

$$\sum \dot{m}_{\text{in}} = \sum \dot{m}_{\text{out}} \quad \text{(kg/s)} \tag{12}$$

$$\dot{Q} - \dot{W} = \sum \dot{m}_{\text{out}}\, h_{\text{out}} - \sum \dot{m}_{\text{in}}\, h_{\text{in}} \quad \text{(kW)} \tag{13}$$

$$\dot{E}_{\text{heat}} - \dot{W} = \sum \dot{E}_{\text{out}} - \sum \dot{E}_{\text{in}} + \dot{E}_{\text{D}} \quad \text{(kW)} \tag{14}$$

where $\dot{Q}$ shows heat input and $\dot{W}$ demonstrates work output, mass flow rate is given as m, h is the enthalpy, in and out are the subscripts for inlet and exit, and $\dot{E}_{\text{D}}$ is the rate of exergy destruction.

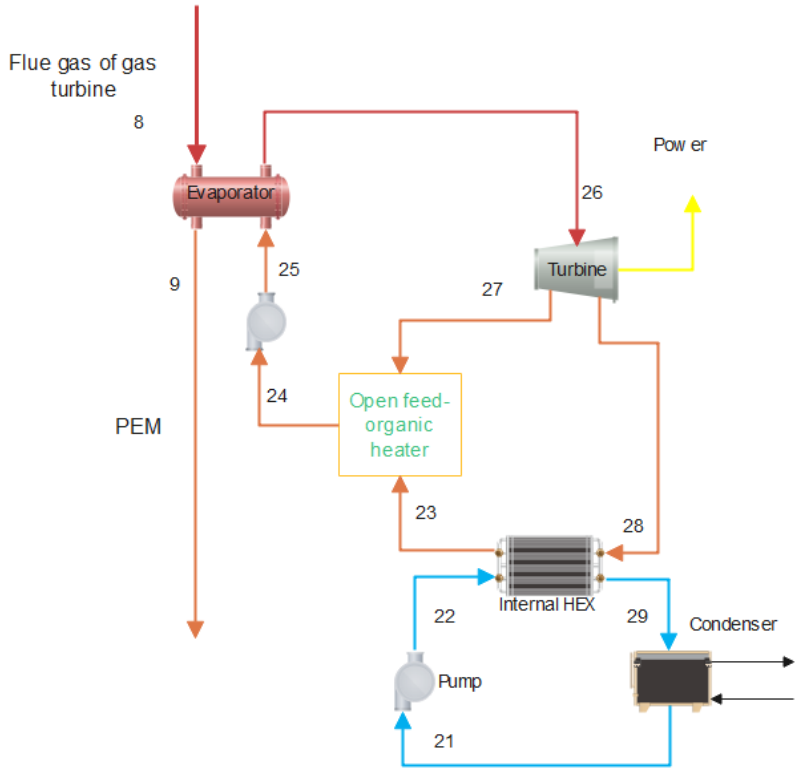

Figure 3.5. Schematic diagram of ORC [14].

Energy and exergy balance equations used in the modelling, for each component of ORC are listed in Table 3.9.

Table 3.9. Energy and exergy balance equations of ORC [21-23].

Subsystems	Energy Relations	Exergy Relations
Pump	$\eta_P = \frac{v_{21}(P_{22} - P_{21})}{h_{22} - h_{21}}$ $= \frac{v_{24}(P_{25} - P_{24})}{h_{25} - h_{24}}, \dot{W}_P$ $= \dot{m}_{25}\left[[(1-y)(h_{22} - h_{21}) + (h_{25} - h_{24})\right]$	$\dot{E}_{D,P} = T_0\dot{m}_{25}[(1-y)(s_{22} - s_{21}) + (s_{25} - s_{24})]$
Evaporator	$\dot{Q}_E = \dot{m}_{25}(h_{26} - h_{25}) = \dot{m}_8(h_8 - h_9)$	$\dot{E}_{D,E} = T_0[\dot{m}_{25}(s_{26} - s_{25}) + \dot{m}_8(s_8 - s_9)]$
Turbine	$\eta_T = \frac{h_{26} - h_{27}}{h_{26} - h_{27s}}$ $= \frac{h_{27} - h_{28}}{h_{27} - h_{28s}}, \dot{W}_T$ $= \dot{m}_{26}[(h_{26} - h_{27}) + (1 - y)(h_{27} - h_{28})]$	$\dot{E}_{D,T} = T_0\dot{m}_{26}[ys_{27} + (1-y)s_{28} - s_{26}]$
OFOH	$y = \frac{h_{24} - h_{23}}{h_{27} - h_{23}}$	$\dot{E}_{D,OFOH} = T_0\dot{m}_{26}[s_{24} - ys_{27} - (1-y)s_{23}]$
IHE	$\varepsilon = \frac{T_{28} - T_{29}}{T_{28} - T_{22}}, Q_{IHE}$ $= \dot{m}_{28}(h_{28} - h_{29})$ $= \dot{m}_{22}(h_{23} - h_{22})$	$\dot{E}_{D,IHE} = T_0[\dot{m}_{22}(s_{22} - s_{23}) + \dot{m}_{28}(s_{29} - s_{28})]$
Condenser	$\dot{Q}_C = \dot{m}_{29}(h_{29} - h_{21}) = \dot{m}_{30}(h_{31} - h_{30})$	$\dot{E}_{D,C} = T_0[\dot{m}_{28}(s_{21} - s_{29}) + \dot{m}_{30}(s_{31} - s_{30})]$

3.2.4. PEM Electrolyzer

The PEM electrolyzer is powered by energy generated by the overall system. The reactions associated with the anode, cathode, and overall form are expressed by Eq.s 15-17 [8].

$$H_2O \rightarrow 2H^+ + 0.5O_2 + 2e^- \quad \text{(Anode side reaction)} \tag{15}$$

$$2H^+ + 2e^- \rightarrow H_2 \quad \text{(Cathode side reaction)} \tag{16}$$

$$H_2O + energy \rightarrow H_2 + 0.5O_2 \quad \text{(Overall reaction)} \tag{17}$$

Hydrogen production rate calculation equation can be expressed by Eq.18.

$$\dot{N}_2 = \frac{J}{2F} \quad \text{(A x mol/cm}^2\text{x C)} \tag{18}$$

F is Faraday constant (C/mol), J is current density (A/cm^2).

Electrical power input to the electrolyzer is calculated using Eq.19:

$$\dot{W}_{PEM} = \frac{\dot{W}_{net}}{2} = JV \quad \text{(kW)} \tag{19}$$

Electrolyzer voltage is described by V and calculated by Eq.20.

$$V = V_0 + V_{act,a} + V_{act,c} + V_{ohm} \quad \text{(V)} \tag{20}$$

Reversible potential (V_0) is determined by Nernst, $V_{act,a}$ and $V_{act,c}$ represents the anode-side, cathode-side activation potential respectively, and ohmic potential is described by V_{ohm} in Eq.21.

$$V_0 = 1.23 - 0.9x\ 10^{-3}(T - 298.15) + 2.3\frac{RT}{4F} lnP_{H_2}^2 P_{O_2} \quad \text{(V)} \tag{21}$$

In Eq.22, R shows universal gas constant (J/mol.K), T describes absolute temperature (K), and $P_{H_2}^2$ and P_{O_2} are hydrogen and oxygen partial pressures (bar), respectively.

The activation potential of the power supply's cathode and anode sides is calculated using Eq.13:

$$V_{act,i} = \frac{R\ x\ T_{PEME}}{F} \sinh^{-1}\left(\frac{J}{2\ x\ J_{0,i}}\right) i = a, c \quad \text{(V)} \tag{22}$$

The electrolyzer exchange current density is denoted by $J_{0,i}$ and is calculated by Eq.23.

$$J_{0,i} = J_i^{ref}\ x \exp\left(-\frac{E_{act,i}}{R\ x\ T_{PEME}}\right), i = a, c \quad \text{(J)} \tag{23}$$

The ohmic potential is also defined as given in Eq.24.

$$V_{ohm} = J\ x\ R_{PEME} \quad \text{(V)} \tag{24}$$

Total ohmic resistance (R_{PEME}) equation is given in Eq.25.

$$R_{PEME} = \int_0^L \frac{dx}{\sigma_{PEME}[\lambda(x)]} \quad \text{(Ohm)} \tag{25}$$

where $\sigma_{PEME}[\lambda(x)]$ and $\lambda(x)$ are the local unique conductivity coefficient and the amount of water at distance x, respectively, and are expressed by Eq.26-27.

$$\sigma_{\mathrm{PEME}}[\lambda(x)] = [0.5139\lambda(x) - 0.326]\left[1268\left(\frac{1}{3P3} - \frac{1}{\mathrm{T_{PEME}}}\right)\right] \tag{26}$$

$$\lambda(x) = \frac{\lambda_2 - \lambda_c}{D} x + \lambda_c \tag{27}$$

Input parameters for modelling of PEM electrolyzer are summarized in Table 3.10.

Table 3.10. Model input parameters of PEM electrolyzer [9, 10].

Parameter	**Unit**	**Value**
P_{O_2}	(bar)	1.0
P_{H_2}	(bar)	1.0
T	(K)	353.15
$E_{activation,anode}$	($kJmol^{-1}$)	76
$E_{activation,cathode}$	($kJmol^{-1}$)	18
λ_{anode}	(Ω^{-1})	14
$\lambda_{cathode}$	(Ω^{-1})	10
L	(m)	$100x10^{-6}$
F	(c mol^{-1})	96,486

3.2.5. Environmental Impact Analysis

Although biomass is a renewable energy source, CO_2 is released from biomass, based on the combustion process and type of the biomass material. The greenhouse gas emissions have penalty cost, and it is directly linked to the CO_2 emissions which are produced annually from the system. The environmental impact cost of CO_2 can be calculated by using Eq.28 [24].

$$\dot{C}_{\text{environmental}} = \dot{m}_{CO_2} C_{CO_2} \tag{28}$$

where $\dot{m}_{CO_2}$ is mass flow rate of CO_2 and C_{CO_2} shows the cost of CO_2 and it is considered as $24\$\ \text{ton}^{-1}$ [25].

3.2.6. Single-Objective Optimization

Single-objective optimization is used to obtain the best operating conditions of a system. Genetic method is selected in EES due to its robustness in the sense that is able to find a global optimum. Following objectives are aimed by optimization via choosing $\dot{m}_{\text{biomass}}$, turbine inlet temperature of gas turbine TIT_{GT} , and TIT_{ORC}.

- Maximization of energy and exergy efficiency
- Minimization of environmental impact

Table 3.11 shows the range of selected parameters. Those limitations are considered based on the biomass availability and component limits during single-objective optimization. $\dot{m}_{\text{biomass}}$, TIT_{GT} (T_6) and (TIT_{ORC}) T_{26} are determined according to turbine material limit based on reference article [26]. When input fresh water mass flow rate increased in PEM electrolyzer (state 33), required power is significantly increased since single-objective optimization is limited up to 0.35 kg/s. The states in Table 3.11 are based on Fig.3.2.

Table 3.11. Upper and lower bounds of selected optimization parameters.

Parameter	$\dot{m}_{\text{biomass}}$ (kg/s)	$\dot{m}_{33}$ (kg/s)	T_6 (°C)	T_{26} (°C)
Lower Bound	4	0.1	1000	100
Upper Bound	10	0.35	1200	160

CHAPTER 4

RESULTS AND DISCUSSIONS

A novel multi-generation system which is powered by biomass and geothermal energy sources of Izmir region, is proposed to increase power generation, efficiency, and production of hydrogen. The proposed multi-generation system includes four subsystems: a BGC, a DFG cycle, an ORC, and a PEM electrolyzer. The system is first modelled for a thorough thermodynamic (energy and exergy) analysis by EES software. The performance parameters for the overall system are determined as generated power, first and second law efficiencies, hydrogen production rates, and the amount of CO_2 emissions. Each subsystem is modelled separately, and the models are validated based on the literature [14, 20, 26]. Table 4.1-4.4 outlines the validation results of BGC, DFG cycle, ORC and PEM electrolyzer, respectively.

Table 4.1. Validation results of BGC model compared with Ref [26].

		Biomass Gasification Cycle	
Parameter	**Unit**	**Present Study**	**Ref [26]**
$\dot{W}_{net}$	kW	23,383	24,218
η_{en}	%	23.36	24.2
η_{ex}	%	22.53	23.1

Table 4.2. Validation results of DFG cycle model compared with Ref [20].

		Double Flash Geothermal Cycle	
Parameter	**Unit**	**Present Study**	**Ref [20]**
η_{en}	%	19.91	17.73
η_{ex}	%	58.63	50.89

Table 4.3. Validation results of ORC model compared with Ref [14].

		Organic Rankine Cycle	
Parameter	**Unit**	**Present Study**	**Ref [14]**
η_{en}	%	18.88	15.35
η_{ex}	%	62.06	52.73

Table 4.4. Validation results of PEM electrolyzer model compared with Ref [26].

		PEM	
Parameter	**Unit**	**Present Study**	**Ref [26]**
η_{en}	%	64.31	64.4
η_{ex}	%	63.6	63.3

The validated subsystem models are used to simulate combined multi-generation system. In addition, a parametric study is performed to determine best operating condition for each subsystem. The assumptions for the parametric study are given in Table 4.5. Furthermore, single-objective optimization is conducted to assess the thermodynamic performance of the multi-generation system under a range of $\dot{m}_{\text{biomass}}$, TIT_{GT} (T_6), TIT_{ORC} (T_{26}) and input fresh water flow rate ($\dot{m}_{33}$) to obtain optimum operating conditions of the overall system. Range of conducted single objective optimization is given in Table 3.11.

Finally, an environmental impact analysis is conducted considering the amount of CO_2 released from the multi-generation system.

Table 4.5. Default parameters for parametric study.

Parameters	**Unit**	**Value**
Ambient temperature, T_0	(◦C)	25
Ambient pressure, P_0	(kPa)	100
	BGC [11]	

(Cont. on next page)

Table 4.5. (Cont.)

Biomass fuel mass flow rate, $\dot{m}_{\text{biomass}}$	(kg/s)	4
Air mass flow rate $\left(=\dot{m}_{\text{GT}}+\dot{m}_{\text{gasifier}}\right), \dot{m}_{\text{air}}$	(kg/s)	56.22 (=54.99 + 1.223)
Pressure ratio, r_{AC}	-	12
Turbine inlet temperature, TIT_{GT}	(°C)	1010
DFG Cycle		
Mass flow rate of geothermal well, $\dot{m}_{10}$	(kg/s)	285
Temperature of throttle valve, T_{10}	(◦C)	237.9
ORC		
Pump inlet temperature	(◦C)	40
Pump pressure ratio		3.75
Heat exchanger turbine inlet temperature, T_{26}	(◦C)	120
Heat exchanger turbine inlet pressure, P_{26}	(kPa)	1201
Steam turbine outlet pressure, P_{27}	(kPa)	581.2
Steam turbine outlet pressure, P_{28}	(kPa)	154.7
PEM Electrolyzer		
Mass flow rate of PEM, $\dot{m}_{33}$	(kg/s)	0.3041
Heat exchanger inlet temperature, T_{33}	(◦C)	25

The properties and quantity of the biomass determine the input energy fed to the overall multi-generation system. Fig.4.1 demonstrates the power output change of each subsystem and overall system with the change of $\dot{m}_{\text{biomass}}$ (4-10 kg/s). This range is determined according to material limits of gas turbine. Biomass flow rate change effects gas turbine flue gas temperature directly. Therefore, it is not suitable to operate the gas turbine above 10 kg/s biomass flow rate. The Figure indicates that increasing $\dot{m}_{\text{biomass}}$ from 4 kg/s to 10 kg/s, increases power output of BGC by 150%. Besides, an increase in $\dot{m}_{\text{biomass}}$ also increases power output of subsystems II and III since the flue gas is the heat source for the rest of the subsystems. Increase in $\dot{m}_{\text{biomass}}$ from 4 kg/s to 10 kg/s caused an increase in overall power generation of the multi-generation system by 74.3%.

Fig.s 4.2 and 4.3 exhibit energy and exergy efficiency changes depending on $\dot{m}_{\text{biomass}}$ change (4-10 kg/s), respectively. In Fig.4.2, a slight energy efficiency increase is observed at DFG (1.3%) while energy efficiency of other subsystems are almost constant. But, an 11.7% increase in energy efficiency is encountered in overall system. Main reason for that, once biomass flow rate increases, produced power of the overall system increases by 75.7% due to biomass cycle. Since flue gas heat content increase during biomass flow rate increase, higher temperature reaches to subsystem II, III. and IV. Higher temperature provides efficiency increase for all subsystems. Besides, this situation leads efficiency increase in PEM electrolyzer. Overall efficiency is calculated considering PEM electrolyzer (63.3%), therefore overall efficiency increase is observed.

In Fig.4.3, it can be observed that exergy efficiency of BGC remains constant with biomass flow rate increase. Exergy efficiency of BGC is calculated power output of BGC divided by biomass mass flow rate times LHV of biomass. Due to linearity, exergy efficiency remains constant. When biomass flow rate increases, mass flow rate of flue gas increases too. Since flue gas has low exergy rate, increasing flue gas flow rate, decreases exergy efficiency of other subsystems and correspondingly overall exergy efficiency decreased by 16.3%.

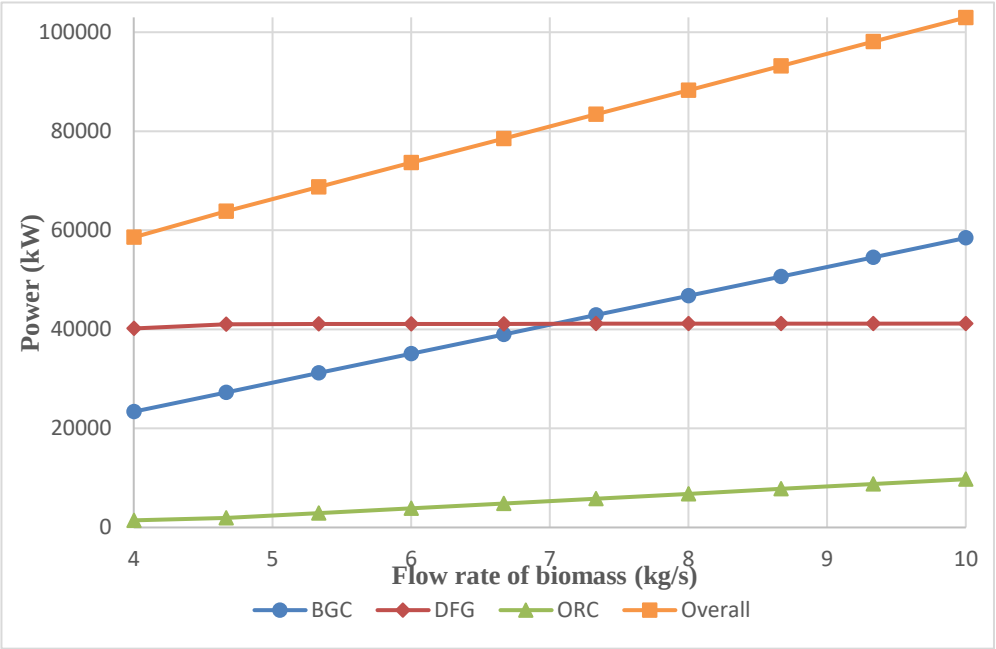

Figure 4.1. Power generation change with biomass flow rate for each subsystem and overall system.

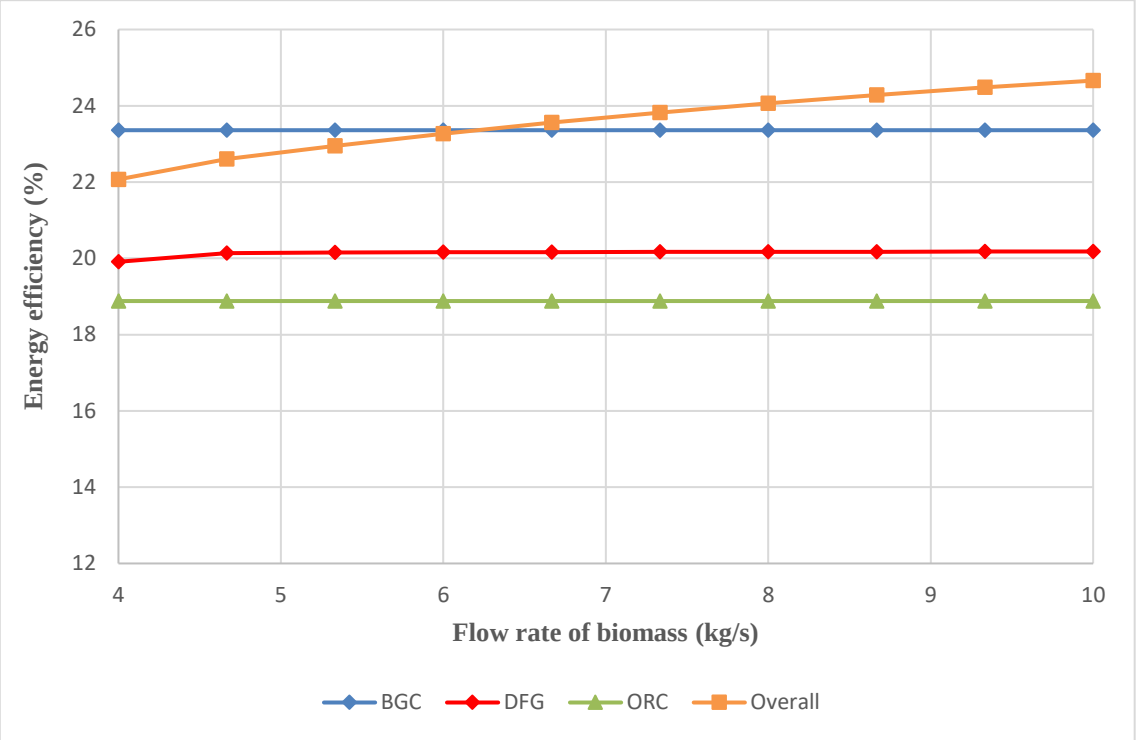

Figure 4.2. Variation of energy efficiency with biomass flow rate for each subsystem and overall system.

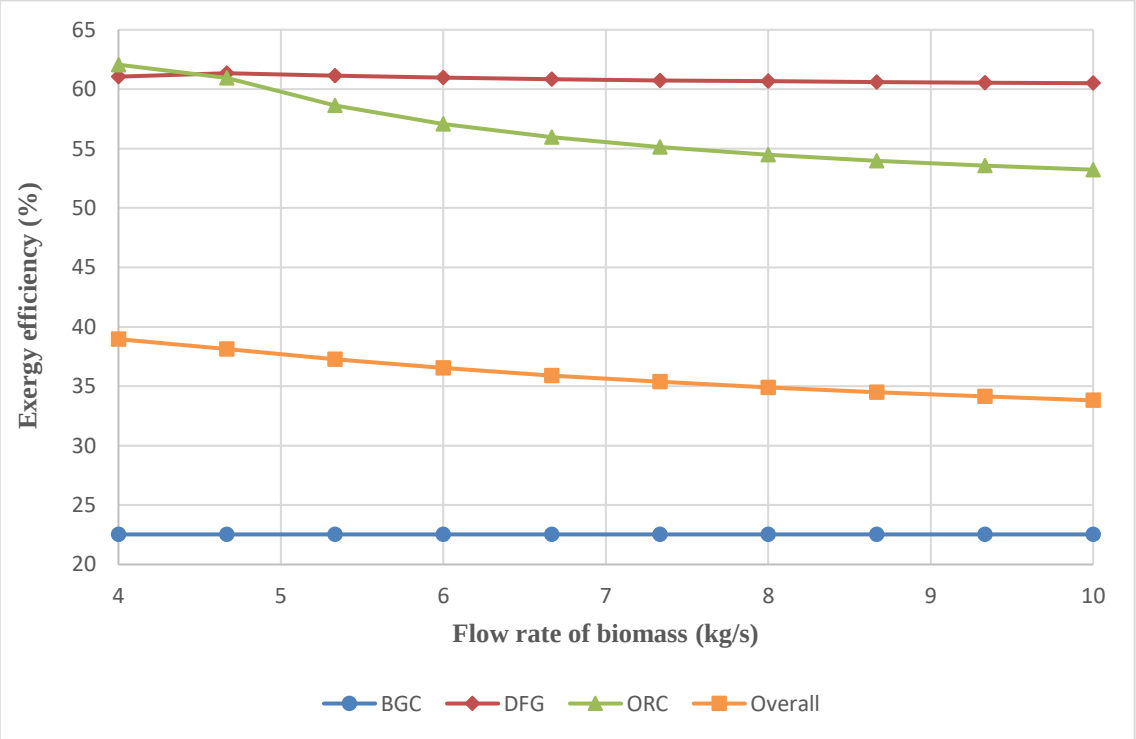

Figure 4.3. Variation of exergy efficiency with biomass flow rate for different subsystems.

Another important parameter, effects the power generation is turbine inlet temperature. Since BGC is dominating on power generation of overall system, first the impact of TIT_{GT} change on energy and exergy efficiencies is evaluated and presented in Fig.s 4.4-4.5. and the , shown. Fig. 4.4 indicates that when TIT_{GT} changes from 1000°C to 1300°C, energy efficiency of BGC (9%), DFG (0.7%) and overall system (4%) increases while ORC efficiency remains constant since turbine inlet temperature is kept constant in ORC

As can be seen from Fig. 4.5, increase in TIT_{GT} leads a 9.1% and 3.9% exergy efficiencies at BGC and overall cycle, respectively. On the other hand, a decrease is encountered in DFG cycle as 1.4% and ORC as 3.7%Since TIT_{GT} is increased, exit temperature of the GT is also increased. This situation leads to exergy efficiency decrease in the subsystem II and III. Besides, even a decrease is observed in these subsystems, overall exergy efficiency is increased because of the higher power output of BGC then other subsystems.

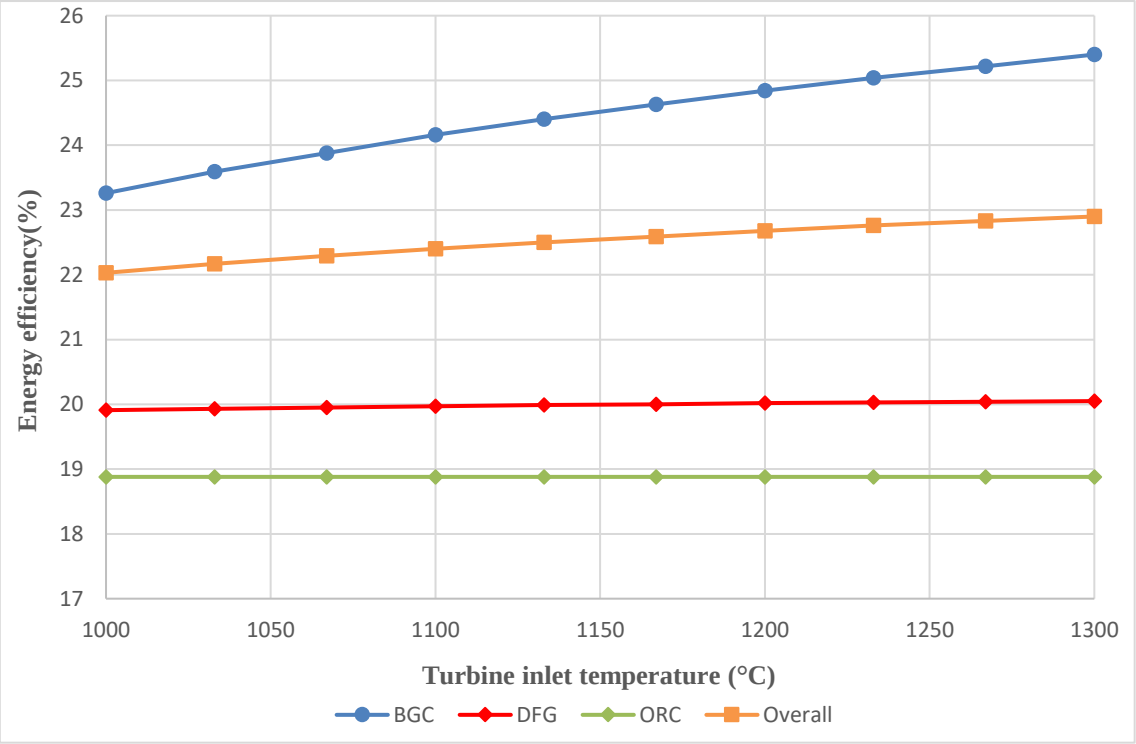

Figure 4.4. Variation of energy efficiency with gas turbine inlet temperature.

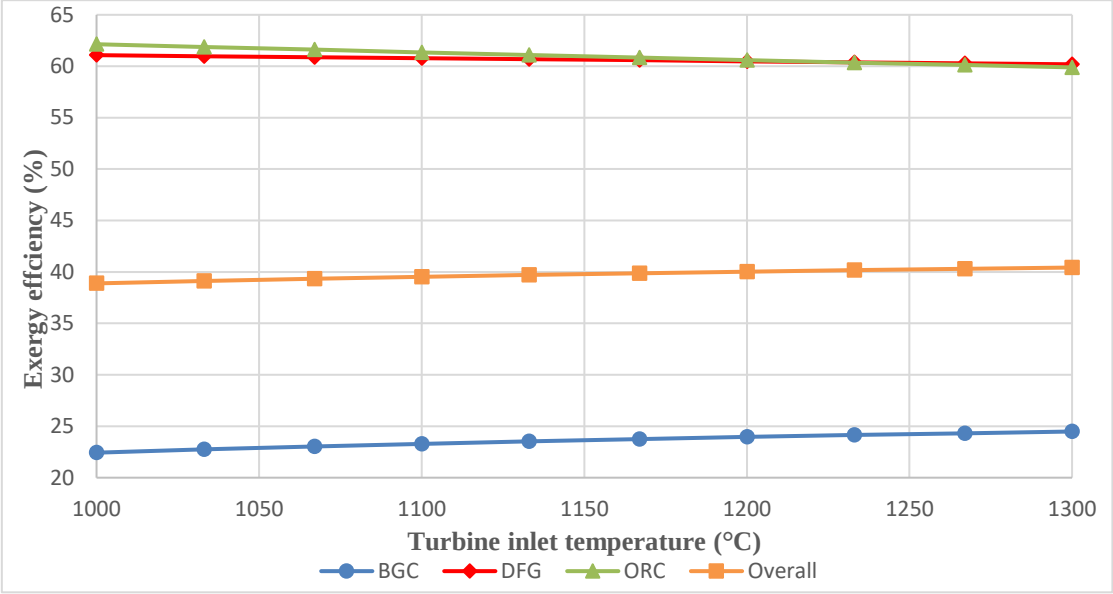

Figure 4.5. Variation of exergy efficiency with gas turbine inlet temperature.

The effect of TIT_{ORC} (T_{26}) (90-175°C) change on energy and exergy efficiencies of the ORC and overall system is shown in Fig. 4.6. The T_{26} has significant effect on energy and exergy efficiencies of ORC as can be seen from the Figure. When T_{26} is increased from 90°C to 175°C, energy and exergy efficiencies of ORC increase by 64.8% and 42.6%, respectively. On the other hand, overall system energy and exergy efficiencies only increase by 1.2%. This result is another indication of CGC dominance on the overall system.

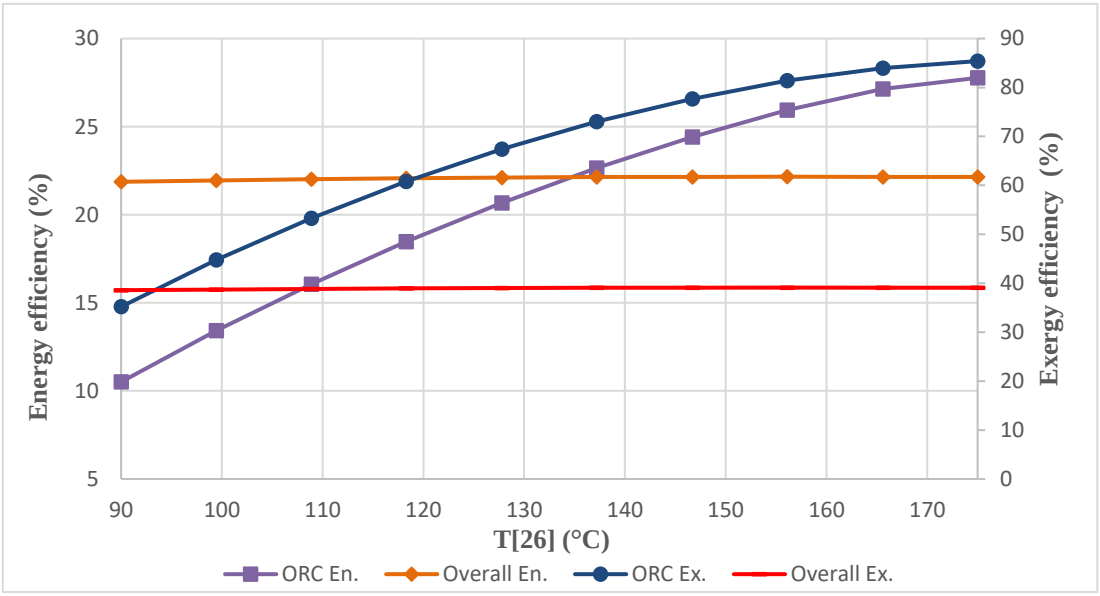

Figure 4.6. Variation of energy and exergy efficiency with ORC turbine inlet temperature.

Fresh water inlet flow rate of the PEM electrolizer is another parameter to be optimized because power consumption of PEM is directly linked with the flow rate. Fig.4.7 shows the change in overall energy and exergy efficiencies, produced amount of H_2 and required power of PEM electrolyzer with the change of fresh water inlet flow rate. When mass flow rate of fresh water rises from 0.1 kg/s to 0.5 kg/s, amount of produced H_2 and required power for the electrolizer increase 400%. In addition, energy and exergy efficiencies of overall multi-generation system are decreased by 5%. The increase in power requirement based on the increase in fresh water flow rate negatively affects the energy and exergy efficiencies of the system since the power input of the PEM electrolizer is provided by the power generation of the overall system.

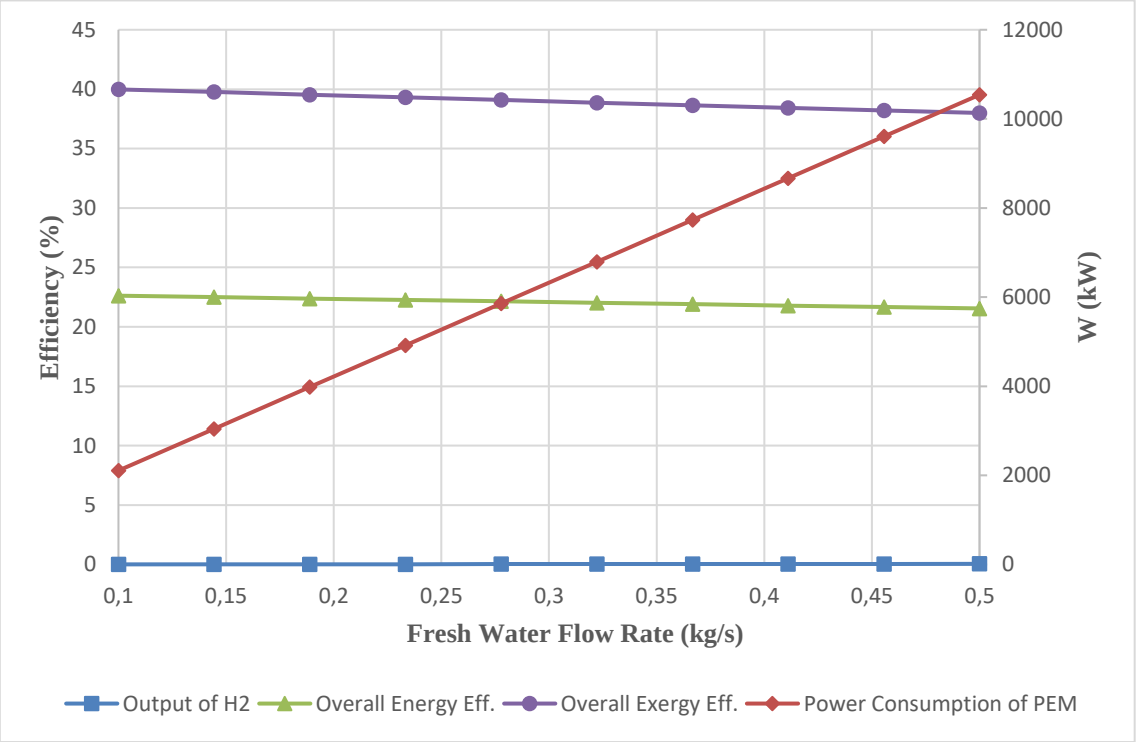

Figure 4.7. Variation of consumed power produced H_2 with inlet fresh water flow rate.

Power generation is highly effected by ambient temperature which is the lowest temperature that a power cycle can operates. The effect of ambient temperature change (-20°C to 50°C) on the energy and exergy efficiencies of multi-generation system and its subsystems are shown in Fig.s 4.8 and 4.9. The BGC and overall system energy efficiency decrease by 0.3%, 8% respectively. In contrast, DFG cycle energy efficiency is slightly increased by 1.8%. Furthermore, from exergy point of view changing the ambient temperature from -20°C to 50°C leads a slight energy efficiency increase on PEM,

geothermal and ORC cycles. On the other hand, variation of T_0 reduces BGC and the multi-generation system's exergy efficiency 0.4%.

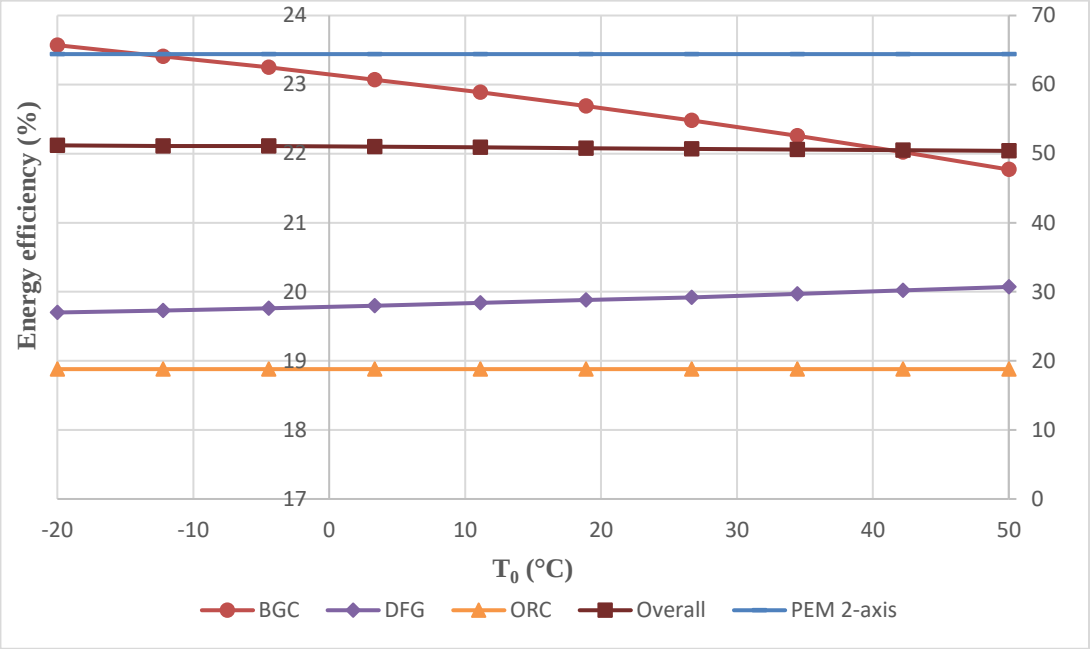

Figure 4.8. Variation of energy efficiency with dead state temperature.

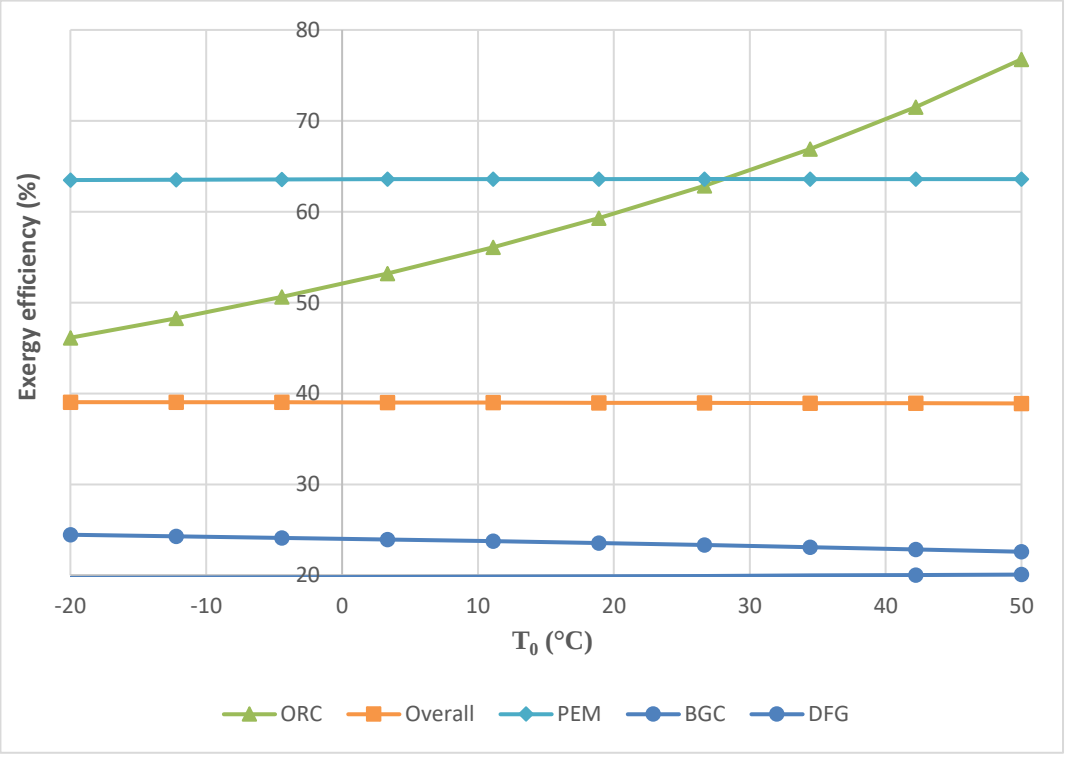

Figure 4.9. Variation of exergy efficiency with dead state temperature.

The Fig.s 4.10-4.12 demonstrate the exergy destruction rates for ORC, DFG, BGC and PEM. Fig. 4.10 exhibits the exergy destruction rates of BGC components. The highest exergy destruction rates are encountered at gasifier as 79% and combustion chamber as 18% because of partial combustion and the chemical reactions.

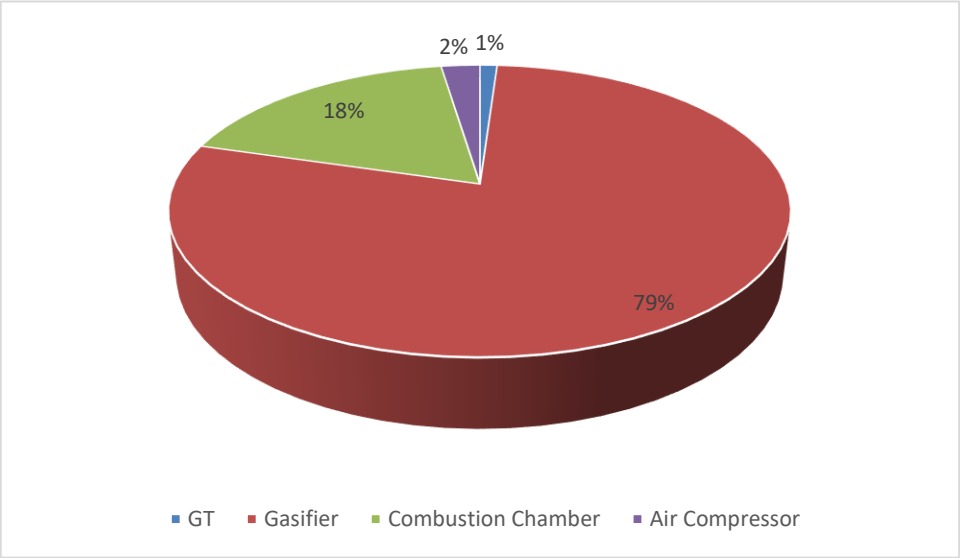

Figure 4.10. Exergy destruction rates of BGC.

Exergy destruction rates for ORC components are given in Fig. 4.11. Evaporator (40%) has the highest share in exergy destruction rate, followed by condenser (32%) and turbine (20%)

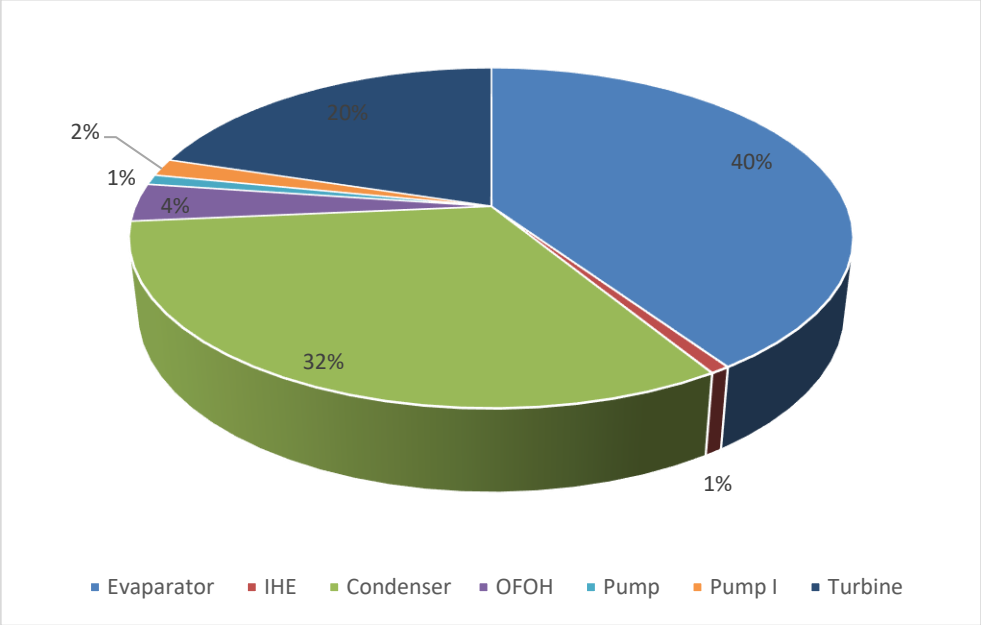

Figure 4.11. Exergy destruction rates of ORC.

Condenser exergy destruction rate (69%) is more obvious (Fig.4.12) in DFG cycle which is the only heat exchanger of the cycle. HP and LP turbines total as 19% exergy destruction rate.

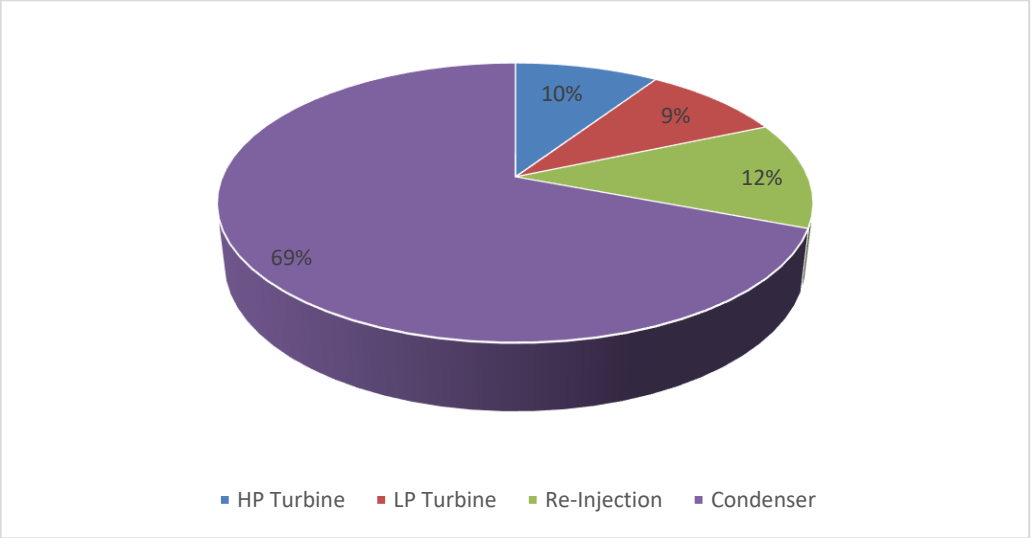

Figure 4.12. Exergy destruction rates of DFG.

Total exergy destruction rates of each subsystem are summarized in Fig.4.13.

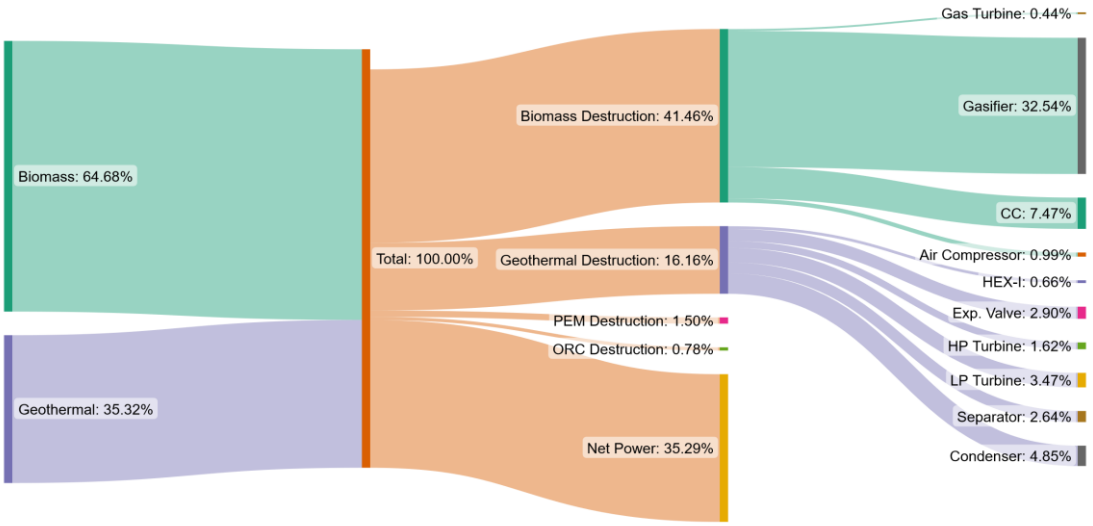

Figure 4.13. Exergy destruction rates of all subsystems.

Besides thermodynamic parameters, environmental parameters are vital on power generation systems. Figure 4.14 shows the effect of changing $\dot{m}_{\text{biomass}}$ from 4 kg/s to 10 kg/s on environmental impact cost of CO_2 for the overall system. It is noted that by rising $\dot{m}_{\text{biomass}}$, environmental impact cost of CO_2 is increased from 2.99 M\$ year $^{-1}$ to 6.98 M\$ year $^{-1}$.

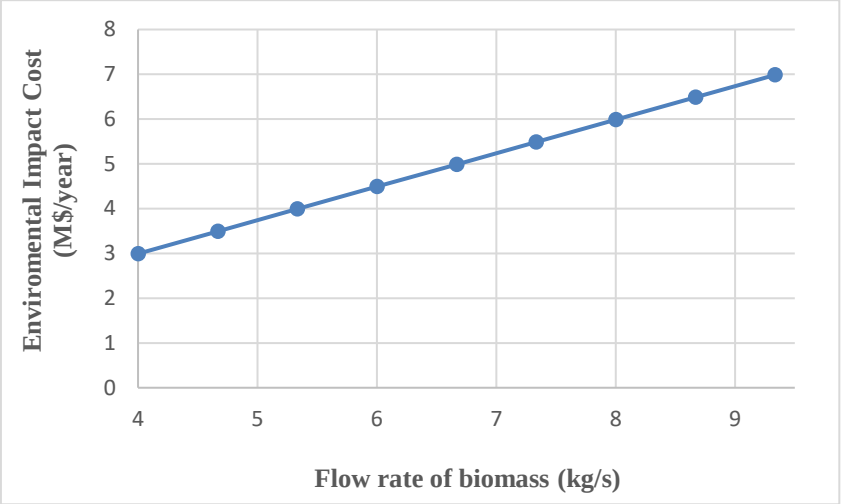

Figure 4.14. Environmental cost change depending on the biomass flow rate.

To obtain optimum operating parameters of the overall system, single-objective analysis is performed for the objectives of maximum energy and exergy efficiencies with minimum environmental impact cost of CO_2. Table 4.6 lists the values of variable parameters which give maximum energy and exergy efficiencies and minimum environmental impact cost of CO_2. Single-objective optimization deals with the maximization or minimization of the parameters based upon a single objective. Therefore, the variables are different for each objective as can be seen from the Table. Multi-objective optimization is the tool that give two or more conflicting objectives are simultaneously optimized with respect to a given set of variables.

Table 4.6 The optimized values for the proposed system.

Parameter	**Unit**	**Maximization of Energy Efficiency**	**Maximization of Exergy Efficiency**	**Minimization of Environmental Impact Cost**
$\dot{m}_{\text{biomass}}$	(kg/s)	9.9	4	4
$\dot{m}_{33}$	(kg/s)	0.129	0.1	0.138
TIT_{GT}	(°C)	1177	1200	1199
T_{26}	(°C)	159.6	156	119.2
η_{en}	(%)	**27.6**	25.5	23.1
η_{ex}	(%)	37.8	**41.2**	40.8
W_{net}	(kW)	117,819	64,999	63,772
Environmental Impact Cost	(M$/year)	7.4	2.9	**2.9**

CHAPTER 5

CONCLUSIONS

The Thesis study aims to ensure the sustainability by increasing overall efficiency and energy output via local energy sources (geothermal energy and biomass) which are abandoned in Izmir Region-Turkiye. A novel multi-generation system is proposed which includes a BGC, a DFG cycle, an ORC and a PEM electrolyzer. The study clearly showed that the waste heat generated by the BGC subsystem is coupled with a DFG cycle, an ORC and a PEM electrolyzer subsystems. Instead of generating power by a single-generation system and reject a high amount of waste heat to the environment, proposed multi-generation system improves energy (55.2%) and exergy efficiencies (17.1%), and power generation (85%) along with valuable market product which is hydrogen with a minimized waste heat.

Thermodynamic and environmental impact assessments, and single-objective optimization are performed to evaluate the proposed system performance while considering working condition of each subsystem. The power output, exergy destruction, energy, and exergy efficiencies and environmental impact cost of CO_2 of each subsystem and overall system are evaluated and discussed.

Some concluding remarks which can be extracted from this study are as follows:

- As a result of the comprehensive exergy analysis, BGC has the largest exergy destruction rate compared to the other subsystems because of the partial combustion and the chemical reactions occur in the combustion chamber of this cycle.
- A 300°C temperature increase at gas turbine inlet from 1000°C to 1300°C leads to 3.9% increase in overall energy efficiency and 1.8% increase in overall exergy efficiency.
- An increase in turbine inlet temperature of ORC from 90°C to 175°C, caused 1.2% increase in overall energy efficiency and 1.3% increase in overall exergy efficiency.

- Increasing biomass flow rate from 4 kg/s to 10 kg/s lead an increase (23.6%) and decrease (13.2%) in overall energy and exergy efficiencies, respectively. Contrary, biomass flow rate increase resulted a 225% increase in environmental faulty cost.

Single-objective optimization results indicated that when the highest energy efficiency is selected as the target, high environmental impact cost occurs, while when the lowest environmental impact cost is selected, the amount of power produced decreases. It can be concluded that single-objective optimization cannot help to determine the best operating conditions. Thus, multi-objective optimization is recommended on determining the optimum operational parameters.

The current research demonstrates the effectiveness of a multi-generation system powered by two-renewable energy sources which are biomass and geothermal. For future studies, another renewable energy sources or waste heat where available can be included to the input energy mix of multi-generation systems for a variety of outputs based on the needs. Since Turkiye has great sea water potential, it might be considered to implement a desalination unit to produce fresh water for hydrogen production instead of using fresh water. Moreover, performing cost analysis for each system and multi-objective optimization analysis will be valuable to determine the best operation conditions considering cost of the system. In this thesis study, approximately 117 MW power is produced. Therefore, from the power engineering point of view, it is also important to study grid integration of multi-generation systems.

REFERENCES

[1] Menendez J, Ordonez A, Alvarez R, Loredo J. Energy from closed mines: Underground energy storage and geothermal applications. Renew Sustain Energy Rev 2019;108:498–512. https://doi.org/10.1016/j.rser.2019.04.007.

[2] Paulillo A, Striolo A, Lettieri P. The environmental impacts and the carbon intensity of geothermal energy: A case study on the Hellisheiði plant. Environ Int 2019;133:105226. https://doi.org/10.1016/j.envint.2019.105226.

[3] World gross electricity production by source, 2019, IEA, Paris https://www.iea.org/data-and-statistics/charts/world-gross-electricity-production-by-source-2019

[4] IEA. Electricity from biomass: from small to large scale. IEA Bioenergy 2013:4–7. ExCo:2015:02.

[5] DOE. Biopower, www.nrel.gov/analysis/power_databook/, (n.d.).

[6] Hu M, Guo D, Ma C, Luo S, Chen X, Cheng Q, et al. A novel pilot-scale production of fuel gas by allothermal biomass gasification using biomass micron fuel (BMF) as external heat source. Clean Technol Environ Policy 2016;18:743–51. https://doi.org/10.1007/s10098-015-1038-2.

[7] Seyboth K. Intergovernmental panel on climate change. Renewable energy sources and climate change mitigation: special report of the intergovernmental panel on climate change. Cambridge University Press; 2012.

[8] Jabbari B, Jalilnejad E, Ghasemzadeh K, Iulianelli A. Recent progresses in application of membrane bioreactors in production of biohydrogen. Membranes (Basel) 2019;9:1–30. https://doi.org/10.3390/membranes9080100.

[9] Ioroi T, Yasuda K, Siroma Z, Fujiwara N, Miyazaki Y. Thin film electrocatalyst layer for unitized regenerative polymer electrolyte fuel cells. J Power Sources 2002;112:583e7. http://dx.doi.org/10.1016/S0378-7753(02)00466-4.

[10] Millet P, Andolfatto F, Durand R. Design and performance of a solid polymer electrolyte water electrolyzer. Int J Hydrogen Energy 1996;21:87e93. http://dx.doi.org/10.1016/0360-3199(95)00005-4.

[11] Srinivas T, Reddy BV, Gupta AVSSKS. Biomass-fuelled integrated power and refrigeration system. Proc Inst Mech Eng Part A J Power Energy 2011;225:249e58. http://dx.doi.org/10.1177/2041296710394284.

[12] Ahmadi P, Dincer I, Rosen MA. Thermodynamic modeling and multi-objective evolutionary-based optimization of a new multigeneration energy system. Energy Convers Manage 2013;76:282e300. http://dx.doi.org/10.1016/j.enconman.2013.07.049.

[13] DiPippo R. Geothermal Power Plants: Principles, Applications, Case Studies and Envirometnal Impact. 2008.

[14] Yari M. Exergetic analysis of various types of geothermal power plants. Renew Energy 2010;35(1):112–21. https://doi.org/10.1016/j.renene.2009.07.023.

[15] DiPippo R. Geothermal double-flash plant with interstage reheating: An updated and expanded thermal and exergetic analysis and optimization. Geothermics 2013; 48:121–31. https://doi.org/10.1016/j.geothermics.2013.07.006

[16] Javadi MA, Ghomashi H. Thermodynamics analysis and optimization of Abadan combined cycle power plant. Indian J Sci Technol 2016;9:60–72.

[17] Bejan A, Tsatsaronis G, Moran MJ. Thermal Design and Optimization 1995;560.

[18] F-Chart (2022). EES: Engineering Equation Solver | F-Chart Software : Engineering Software. Retrieved 21 November 2022, from https://fchartsoftware.com/ees/

[19] Javadi, M., Khalili Abhari, M., Ghasemiasl, R., & Ghomashi, H. (2021). Energy, exergy and exergy-economic analysis of a new multigeneration system based on double-flash geothermal power plant and solar power tower. Sustainable Energy Technologies And Assessments, 47, 101536. doi: 10.1016/j.seta.2021.101536

[20] Mohammadzadeh Bina, S., Jalilinasrabady, S., Fujii, H. (2018). Exergoeconomic

analysis and optimization of single and double flash cycles for Sabalan Geothermal Power Plant. Geothermics, 72, 74–82. doi: 10.1016/j.geothermics.2017.10.013

[21] Yari M. Performance analysis of the different organic Rankine cycles (ORCs) using dry fluids. International Journal of Exergy 2009;6(3):323–42.

[22] Cengel YA, Boles MA. Thermodynamics: an engineering approach. 6th ed. New York: McGraw-Hill; 2007.

[23] Yari M, Zarin A, Shaker H. Exergetic performance comparison of various type geothermal power plants. In: Proceedings of global conference on global warming, GCGW08, Istanbul, Turkey; July 6–10, 2008.

[24] Mosaffa AH, Farshi LG, Infante Ferreira CA, Rosen MA. Exergoeconomic and environmental analyses of CO_2/NH3 cascade refrigeration systems equipped with different types of flash tank intercoolers. Energy Convers Manag 2016;117:442e53. http://dx.doi.org/10.1016/j.enconman.2016.03.053.

[25] Rubin ES, Davison JE, Herzog HJ. The cost of CO_2 capture and storage, Int. J Greenh Gas Control 2015;40:378e400. http://dx.doi.org/10.1016/j.ijggc.2015.05.018.

[26] Taheri, M.H., Mosaffa, A.H. and Farshi, L.G. (2017) “Energy, Exergy and economic assessments of a novel integrated biomass based multigeneration energy system with hydrogen production and LNG Regasification Cycle,” Energy, 125, pp. 162–177. Available at: https://doi.org/10.1016/j.energy.2017.02.124.

[27] Bejan A, Tsatsaronis G, Moran MJ. Thermal design and optimization. Wiley;1996.

[28] Koponen J, Kosonen A, Ruuskanen V, Huoman K, Niemelä M, Ahola J. Control and energy efficiency of PEM water electrolyzers in renewable energy systems. Int J Hydrogen Energy 2017;2.. https://doi.org/10.1016/j.ijhydene.2017.10.056.

[29] Karapekmez, A., & Dincer, I. (2020). Thermodynamic analysis of a novel solar and geothermal based combined energy system for hydrogen production. International Journal of Hydrogen Energy, 45(9), 5608–5628.

https://doi.org/10.1016/j.ijhydene.2018.12.046

[30] Ahmadi, P., Dincer, I., & Rosen, M. A. (2013). Development and assessment of an integrated biomass-based multi-generation energy system. Energy, 56, 155–166. https://doi.org/10.1016/j.energy.2013.04.024

[31] Ozturk, M. (2017). Energy and exergy analysis of renewable energy sources based integrated system for multi-generation application. International Journal of Exergy, 22(1), 1. https://doi.org/10.1504/ijex.2017.10003719

[32] Koc, M., Yuksel, Y.E. and Ozturk, M. (2022) “Thermodynamic and Exergo-economic assessments of a new geothermally driven multigeneration plant,” International Journal of Hydrogen Energy, 47(45), pp. 19463–19480. Available at: https://doi.org/10.1016/j.ijhydene.2022.01.044.